Tuning entanglement and ergodicity in two-dimensional spin systems using impurities and anisotropy

Gehad Sadiek,[1,*] Qing Xu,[2] and Sabre Kais[2]
[1]*Department of Physics, King Saud University, Riyadh 11451, Saudi Arabia and Department of Physics, Ain Shams University, Cairo 11566, Egypt*
[2]*Department of Chemistry and Birck Nanotechnology Center, Purdue University, West Lafayette, Indiana 47907, USA*
(Received 29 December 2011; published 13 April 2012)

We consider the entanglement in a two-dimensional XY model in an external magnetic field h. The model consists of a set of seven localized spin-$\frac{1}{2}$ particles in a two-dimensional triangular lattice coupled through nearest-neighbor exchange interaction J. We examine the effect of single and double impurities in the system as well as the degree of anisotropy on the nearest-neighbor entanglement and ergodicity of the system. We have found that the entanglement of the system at the different degrees of anisotropy mimics that of the one-dimensional spin systems at the extremely small and large values of the parameter $\lambda = h/J$. The entanglement of the Ising and partially anisotropic systems shows phase transition in the vicinity of $\lambda = 2$, whereas, the entanglement of the isotropic system suddenly vanishes there. Also, we investigate the dynamic response of the system containing single and double impurities to an external exponential magnetic field at different degrees of anisotropy. We have demonstrated that the ergodicity of the system can be controlled by varying the strength and location of the impurities as well as the degree of anisotropy of the coupling.

DOI: 10.1103/PhysRevA.85.042313 PACS number(s): 03.67.Mn, 03.65.Ud, 75.10.Jm, 73.43.Nq

I. INTRODUCTION

Quantum entanglement is a cornerstone in the structure of quantum theory with no classical analog [1]. Entanglement is a nonlocal correlation between two (or more) quantum systems such that the description of their states has to be done with reference to each other even if they are spatially well separated. Particular fields where entanglement is considered as a crucial resource are quantum teleportation, cryptography, and quantum computation [2,3] where it provides the physical basis for manipulating the linear superposition of the quantum states used to implement the different computational algorithms. On the other hand, many questions regarding the behavior of the complex quantum systems significantly rely on a deep understanding and a good quantification of the entanglement [4–9]. Particularly, entanglement is considered as the physical resource responsible for the long-range correlations taking place in many-body systems during quantum phase transitions. There has been great interest in studying the different sources of errors in quantum computing and their effect on quantum gate operations [10,11]. Different approaches have been proposed for protecting quantum systems during the computational implementation of algorithms, such as quantum error correction [12] and decoherence-free subspace [13,14]. Nevertheless, realizing a practical protection against the different types of induced decoherence is still a hard task. Therefore, studying the effect of naturally existing sources of errors, such as impurities and lack of isotropy in coupling between the quantum systems implementing the quantum computing algorithms, is a must. Furthermore, considerable efforts should be devoted to utilizing such sources to tune the entanglement rather than eliminating them. The effect of impurities and anisotropy of coupling between neighbor spins in a one-dimensional (1D) spin system has been investigated [15]. It was demonstrated that the entanglement can be tuned in a class of one-dimensional systems by varying the anisotropy of the coupling parameter as well as by introducing impurities into the spin system. For a physical quantity to be eligible for an equilibrium statistical mechanical description, it has to be ergodic, which means that its time average coincides with its ensemble average. To test ergodicity for a physical quantity, one has to compare the time evolution of its physical state to the corresponding equilibrium state. There has been an intensive effort to investigate ergodicity in one-dimensional spin chains where it was demonstrated that the entanglement, magnetization, and spin-spin correlation functions are nonergodic in Ising and XY spin chains for a finite number of spins as well as at the thermodynamic limit [8,16–18].

Studying quantum entanglement in two-dimensional systems faces more obstacles in comparison to the one-dimensional case, particularly, the rapid increase in the dimension of the Hilbert spaces, which lead to much larger scale calculations relying mainly on the numerical methods. The existence of exact solutions has contributed enormously to the understanding of the entanglement for 1D systems [8,18–20]. In a previous paper, the entanglement in a 19-site two-dimensional transverse Ising model at zero temperature [21] was studied. The spin-$\frac{1}{2}$ particles are coupled through an exchange interaction J and are subject to an external time-independent magnetic field h. It was demonstrated that, for such a class of systems, the entanglement can be tuned by varying the parameter $\lambda = h/J$ and by introducing impurities into the system, which showed a quantum phase transition at a critical value of the parameter λ in the vicinity of 2. Recently, we have investigated the time evolution of entanglement in a two-dimensional triangular transverse Ising system with seven spins in an external magnetic field [22]. Different time-dependent forms of the magnetic field were applied. The systems have demonstrated different responses based on the

*Corresponding author: gehad@ksu.edu.sa

type of applied field where, for a smoothly changing magnetic field, the system entanglement follows the profile of the field very closely.

In this paper, we consider the entanglement in a two-dimensional XY triangular spin system where the nearest-neighbor spins are coupled through an exchange interaction J and are subject to an external magnetic field h. We consider the system at different degrees of anisotropy to test its effect on the system entanglement and dynamics. The number of spins in the system is 7 with a number of impurities existing. We consider two different cases of impurities, the first case is a single impurity existing either at the border of the system or at the center with the coupling strength between the impurity spin and its neighbors different from that between the rest of the spins. The second case is double impurities, existing both at the border or one at the border and one at the center. We consider the coupling between the two impurities as J', which is different from the coupling J'' between each one of them and its neighbors, while the interaction among the other spins is J.

We show that the entanglement profile of the system at different degrees of anisotropy has great resemblance to that of the one-dimensional spin systems as the parameter $\lambda \to 0$ and ∞. On the other hand, both the Ising and the partially anisotropic systems show phase transition behavior in the vicinity of $\lambda = 2$, but the isotropic system shows sharp step variations in the same region before suddenly vanishing. Examining the effect of an external exponential magnetic field on the time evolution of the entanglement showed that the ergodicity of the system can be tuned by varying the strength and location of the impurities and the degree of anisotropy in the system.

This paper is organized as follows. In the next section, we present our model and quantification of entanglement. In Sec. III, we consider the case of a single impurity. In Sec. IV, we study the system with a double impurity. We conclude in Sec. V.

II. MODEL AND QUANTIFICATION OF ENTANGLEMENT

We consider a set of seven localized spin-$\frac{1}{2}$ particles in a two-dimensional triangular lattice coupled through exchange interaction J and subject to an external time-dependent magnetic field of strength $h(t)$ (see Fig. 1). All the particles are identical except one (or two) of them, which are considered

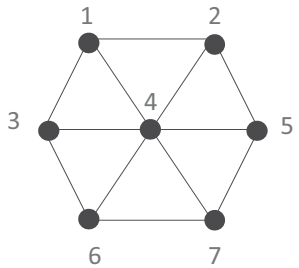

FIG. 1. The two-dimensional triangular spin lattice in the presence of an external transverse magnetic field.

impurities. The Hamiltonian for such a system is given by

$$H = -\frac{(1+\gamma)}{2}\sum_{\langle i,j\rangle} J_{i,j}\sigma_i^x\sigma_j^x - \frac{(1-\gamma)}{2}\sum_{\langle i,j\rangle} J_{i,j}\sigma_i^y\sigma_j^y - h(t)\sum_i \sigma_i^z, \quad (1)$$

where $\langle i,j\rangle$ is a pair of nearest-neighbor sites on the lattice $J_{i,j} = J$ for all sites except the sites nearest to an impurity site. For a single impurity, the coupling between the impurity and its neighbors is $J_{i,j} = J' = (\alpha+1)J$, where α measures the strength of the impurity. For double impurities, $J_{i,j} = J' = (\alpha_1+1)J$ is the coupling between the two impurities, and $J_{i,j} = J'' = (\alpha_2+1)J$ is the coupling between any one of the two impurities and its neighbors, whereas, the coupling is just J between the rest of the spins.

For this model, it is convenient to set $J = 1$. For a system of seven spins, its Hilbert space is huge with 2^7 dimensions, yet it is exactly diagonalizable using the standard computational techniques. Exactly solving the Schrödinger equation of the Hamiltonian (1) yields the system energy eigenvalues E_i and eigenfunctions ψ_i. The density matrix of the system is defined by

$$\rho = |\psi_0\rangle\langle\psi_0|, \quad (2)$$

where $|\psi_0\rangle$ is the ground-state energy of the entire spin system. We confine our interest to the entanglement between two spins at any sites i and j [23]. All the information needed in this case, at any moment t, is contained in the reduced density matrix $\rho_{i,j}(t)$, which can be obtained from the entire system density matrix by integrating out all the spin states except i and j. We adopt the entanglement of formation as a well-known measure of entanglement where Wootters [24] has shown that, for a pair of binary qubits, the concurrence C, which goes from 0 to 1, can be taken as a measure of entanglement. The concurrence between two sites i and j is defined as

$$C(\rho) = \max\{0,\epsilon_1 - \epsilon_2 - \epsilon_3 - \epsilon_4\}, \quad (3)$$

where the ϵ_i's are the eigenvalues of the Hermitian matrix $R \equiv \sqrt{\sqrt{\rho}\tilde{\rho}\sqrt{\rho}}$ with $\tilde{\rho} = (\sigma^y \otimes \sigma^y)\rho^*(\sigma^y \otimes \sigma^y)$ and σ^y is the Pauli matrix of the spin in the y direction. For a pair of qubits, the entanglement can be written as

$$E(\rho) = \epsilon(C(\rho)), \quad (4)$$

where ϵ is a function of the concurrence C,

$$\epsilon(C) = h\left(\frac{1-\sqrt{1-C^2}}{2}\right), \quad (5)$$

where h is the binary entropy function,

$$h(x) = -x\,\log_2 x - (1-x)\log_2(1-x). \quad (6)$$

In this case, the entanglement of formation is given in terms of another entanglement measure, the concurrence C. The dynamics of entanglement is evaluated using the same techniques applied in our previous paper [22]. Specifically, we apply the step-by-step time-evolution projection technique, which was proved to give the same exact result as the

matrix transformation technique where both techniques were introduced in Ref. [22] but 20 times faster. In this technique, we assume that our system is initially at t_0 in the ground state at zero temperature $|\phi\rangle$ with energy, say, ε in an external magnetic field with strength a. The magnetic field is turned to a new value b, and the system Hamiltonian becomes H with N eigenpairs E_i and $|\psi_i\rangle$. The original state $|\phi\rangle$ can be expanded in the basis $\{|\psi_i\rangle\}$,

$$|\phi\rangle = c_1|\psi_1\rangle + c_2|\psi_2\rangle + \cdots + c_N|\psi_N\rangle, \tag{7}$$

where

$$c_i = \langle\psi_i|\phi\rangle. \tag{8}$$

When H is independent of time between t and t_0, then we can write

$$\begin{aligned} U(t,t_0)\left|\psi_{i,t_0}\right\rangle &= e^{-iH(t>t_0)(t-t_0)/\hbar}\left|\psi_{i,t_0}\right\rangle \\ &= e^{-iE_i(t-t_0)/\hbar}\left|\psi_{i,t_0}\right\rangle, \end{aligned} \tag{9}$$

where $U(t,t_0)$ is the time-evolution operator. The ground state will evolve with time as

$$\begin{aligned} |\phi(t)\rangle &= c_1|\psi_1\rangle e^{-iE_1(t-t_0)} + c_2|\psi_2\rangle e^{-iE_2(t-t_0)} + \cdots \\ &\quad + c_N|\psi_N\rangle e^{-iE_N(t-t_0)} \\ &= \sum_{i=1}^{N} c_i|\psi_i\rangle e^{-iE_i(t-t_0)}, \end{aligned} \tag{10}$$

and the pure state density matrix becomes

$$\rho(t) = |\phi(t)\rangle\langle\phi(t)|. \tag{11}$$

Simply, any complicated function can be treated as a collection of step functions. When the state evolves to the next step, just repeat the procedure to get the next step results. Of course, the lack of smoothness in the magnetic-field function imposes a challenging obstacle in the calculations, but this can be overcome by choosing a proper small enough time step. Because the size of our seven-site system was still manageable, in our actual calculations, we included all the $2^7 = 128$ states in every step, without any truncation of the higher-energy eigenstates. This ensures us no approximation in this step. But the method itself is aiming at larger size systems, such as the 19-site XY model. By then, due to the computation limit, cutting off higher-energy eigenstates might be a necessary action.

III. SINGLE IMPURITY

A. Static system with border impurity

We define a dimensionless coupling parameter $\lambda = h/J$, and we set $J = 1$ throughout this paper for convenience. We start by considering the effect of a single impurity located at border site 1. The concurrence between impurity site 1 and site 2, $C(1,2)$, versus the parameter λ for the three different models, Ising ($\gamma = 1$), partially anisotropic ($\gamma = 0.5$), and isotropic XY ($\gamma = 0$) at different impurity strengths ($\alpha = -0.5, 0, 0.5, 1$) is in Fig. 2. First, the impurity parameter α is set at zero. For the corresponding Ising model, the concurrence $C(1,2)$ in Fig. 2(a) demonstrates the usual phase transition behavior where it starts at zero value and increases gradually as λ increases reaching a maximum at $\lambda \approx 2$ then decays as

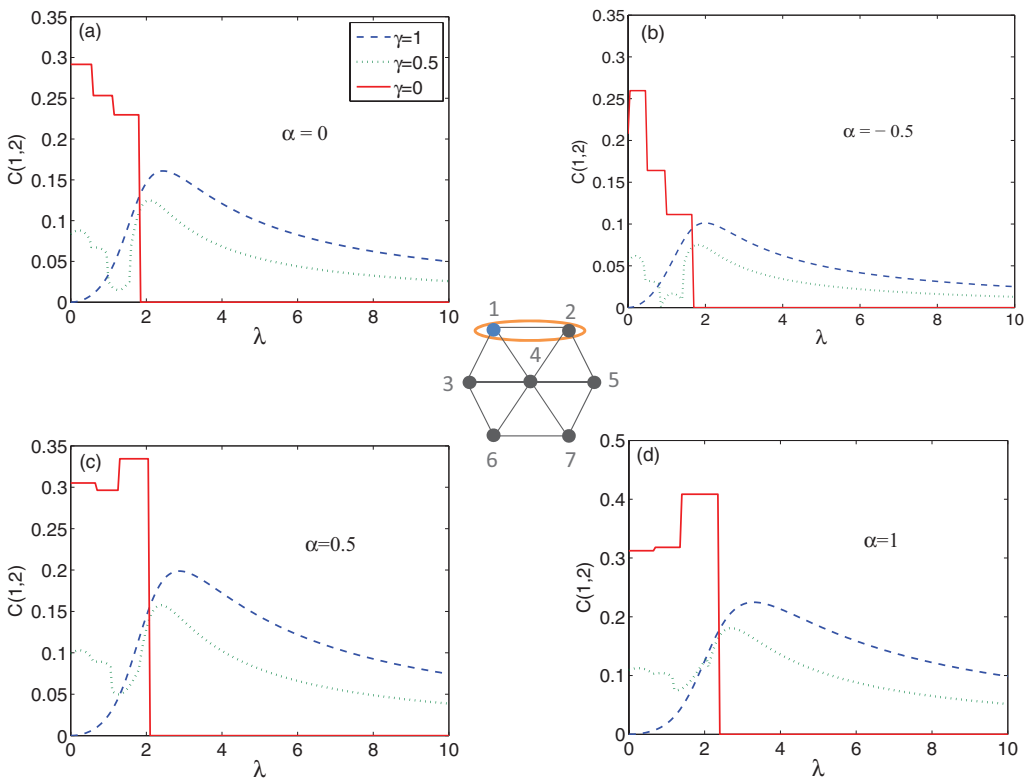

FIG. 2. (Color online) The concurrence $C(1,2)$ versus the parameter λ with a single impurity at border site 1 with different impurity coupling strengths $\alpha = -0.5, 0, 0.5, 1$ for different degrees of anisotropy $\gamma = 1, 0.5, 0$ as shown in the subfigures. The legend for all subfigures is as shown in (a).

λ increases further. As the degree of anisotropy decreases, the behavior of the entanglement changes where it starts with a finite value at $\lambda = 0$ and then shows a step profile for the small values of λ. For the partially anisotropic case, the step profile is smooth, and the entanglement mimics the Ising case as λ increases but with smaller magnitude. The entanglement of the isotropic XY system shows a sharp step behavior then suddenly vanishes before reaching $\lambda = 2$. Interestingly, the entanglement behavior of the two-dimensional spin system at the different degrees of anisotropy mimics the behavior of the one-dimensional spin system at the same degrees of anisotropy at the extreme values of the parameter λ. The ground state of the one-dimensional Ising model is characterized by a quantum phase transition that takes place at the critical value $h/J = 1$ [5,8], which corresponds to a maximum entanglement in the system. The order parameter is the magnetization $\langle \sigma^x \rangle$, which is different from zero for $J \geqslant h$ and zero otherwise. The ground state is paramagnetic when $J/h \to 0$ where the spins get aligned in the magnetic-field direction, the z direction. It is ferromagnetic when $J/h \to \infty$ where the spins are aligned in the x direction. Both cases cause zero entanglement. Comparing the entanglement behavior in the two-dimensional Ising spin system with the one-dimensional system, one can see a great resemblance except that the critical value becomes $h/J \approx 2$ in the two-dimensional case as shown in Fig. 2. On the other hand, for the partially anisotropic and isotropic XY systems, the entanglement of the two-dimensional and one-dimensional systems agrees at the extreme values of λ where it vanishes for $h \gg J$ and reaches a finite value for $h \ll J$. The former case corresponds to an alignment of the spins in the z direction, paramagnetic state, whereas, the latter case corresponds to alignment in the x and y directions, which is a ferromagnetic state.

The effect of a weak impurity ($J' < J$), $\alpha = -0.5$, is shown in Fig. 2(b) where the entanglement behavior is the same as before except that the entanglement magnitude is reduced compared with the pure case. On the other hand, considering the effect of a strong impurity ($J' > J$) where $\alpha = 0.5$ and 1 as shown in Figs. 2(c) and 2(d), respectively, one can see that the entanglement profile for $\gamma = 1$ and 0.5 have the same overall behavior as in the pure and weak impurity cases except that the entanglement magnitude becomes higher as the impurity gets stronger and the peaks shift toward higher λ values. Nevertheless, the isotropic XY system behaves differently from the previous cases where it starts to increase first in a step profile before suddenly dropping to zero again, which will be explained later. To study the entanglement between two sites, none of them is impurity, we consider $C(2,4)$, which is depicted in Fig. 3. There are two main differences between the behavior of $C(2,4)$ and $C(1,2)$. First, the magnitude of the entanglement envelope is higher for $C(2,4)$ for $\gamma = 0.5$ and 0 (but not $\gamma = 1$) when $\alpha = 0$, while $C(2,4)$ is greater than $C(1,2)$ for all γ values for the weak impurity case $\alpha = 0$. This is an interesting result as internal site entanglement should be smaller in value than the edge sites. Second, the entanglement of the isotropic XY case increases in a multistep profile for all values of α before suddenly dropping to zero.

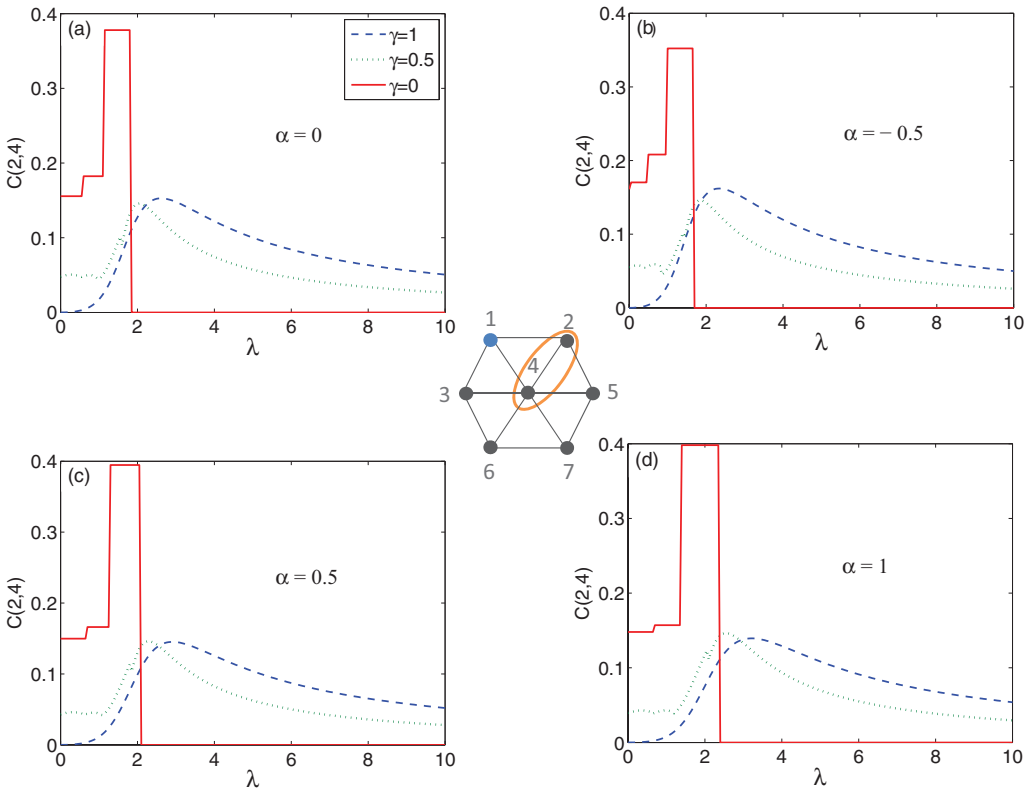

FIG. 3. (Color online) The concurrence $C(2,4)$ versus the parameter λ with a single impurity at border site 1 with different impurity coupling strengths $\alpha = -0.5, 0, 0.5, 1$ for different degrees of anisotropy $\gamma = 1, 0.5, 0$ as shown in the subfigures. The legend for all subfigures is as shown in (a).

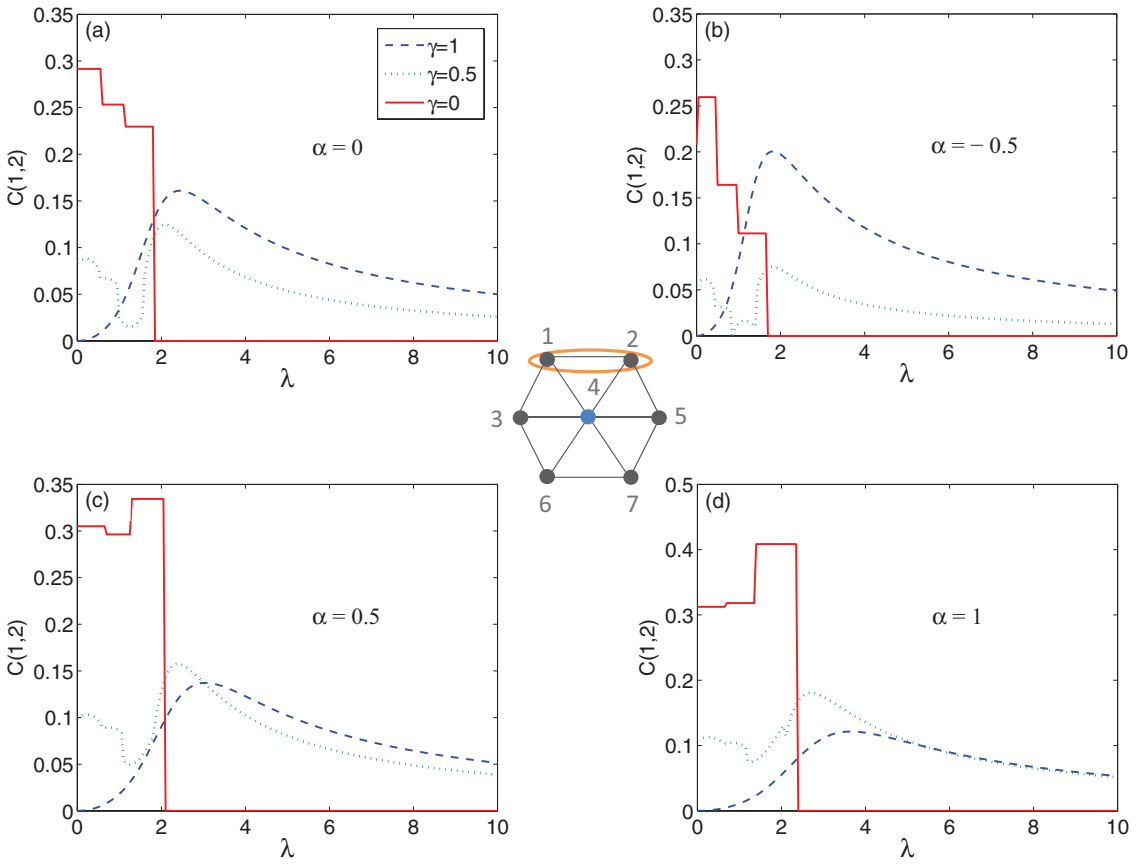

FIG. 4. (Color online) The concurrence $C(1,2)$ versus the parameter λ with a single impurity at central site 4 with different impurity coupling strengths $\alpha = -0.5,0,0.5,1$ for different degrees of anisotropy $\gamma = 1,0.5,0$ as shown in the subfigures. The legend for all subfigures is as shown in (a).

B. Static system with center impurity

To explore the effect of the impurity location, we investigate the case of a single impurity spin located at site 4, instead of site 2, where we plot the concurrences $C(1,2)$ and $C(1,4)$ in Figs. 4 and 5, respectively. Interestingly, while changing the impurity location has almost no effect on the behavior of the entanglement $C(1,2)$ of the partially anisotropic and isotropic XY systems, it has a great impact on that of the Ising system where the peak value of the entanglement increases significantly in the weak impurity case and decreases as the impurity gets stronger as shown in Fig. 4. Now, considering the entanglement between the central impurity site 4 and the edge site 1 and comparing with the results in Fig. 3 of the entanglement between edge site 2 and central site 4, one can see that the entanglement $C(1,4)$ profile for all degrees of anisotropy is very close to $C(2,4)$. Nevertheless, the entanglement $C(1,4)$ magnitude was lower for the weak impurity case and higher for the strong impurity, which meant that the central impurity made a significant change in the entanglement magnitude.

C. Effect of system energy gap on entanglement

To explain the distinct behavior of the entanglement corresponding to the different degrees of anisotropy γ, we depict the lowest few energy eigenvalues of the system at the different γ values for the two cases of border and central impurities in Figs. 6 and 7, respectively. As can be noticed in Fig. 6(a), the energies of the ground state and the first excited state of the Ising system coincide at the beginning at the small values of λ until a specific value where they deviate from each other. This is corresponding to the transition from the degenerated ground state to the nondegenerated one, from paramagnetic to ferromagnetic order by breaking the Z_2 symmetry, which explains the phase transition curve observed in the Ising case. The energy spectrum of the partially anisotropic XY system is a little bit different at the small values of λ where the ground state and the first excited state coincide at the beginning but then deviate slightly from each other before recombining again and, at last, separating from each other completely; this behavior is repeated quite a few times depending on the impurity strength as illustrated in Fig. 6(b). This energy spectrum behavior explains the roughness in the ascending part of the entanglement curves of the partially anisotropic XY system corresponding to subsequent transitions between the ground state and the first excited state taking place before reaching the maximum entanglement point. In Fig. 6(c), the energy spectrum of the isotropic XY system is explored where clearly the deviations and recombination between the ground- and the first excited-state energies become sharper and more frequent compared with the partially anisotropic system. This

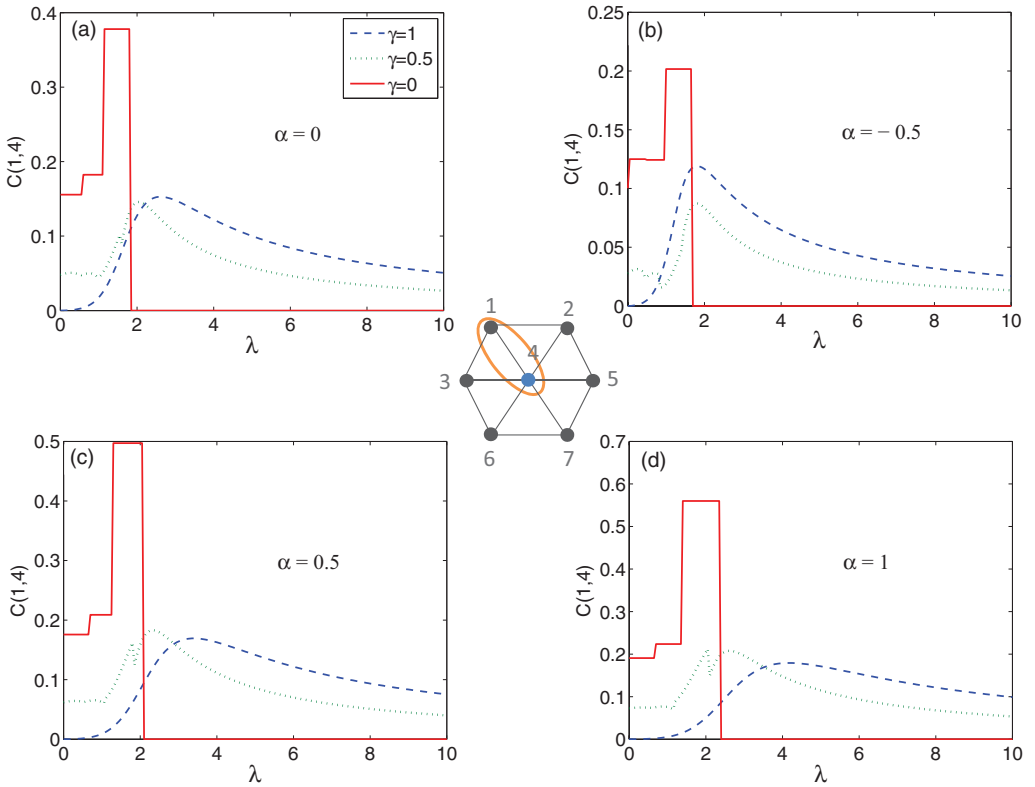

FIG. 5. (Color online) The concurrence $C(1,4)$ versus the parameter λ with a single impurity at border site 4 with different impurity coupling strengths $\alpha = -0.5,0,0.5,1$ for different degrees of anisotropy $\gamma = 1,0.5,0$ as shown in the subfigures. The legend for all subfigures is as shown in (a).

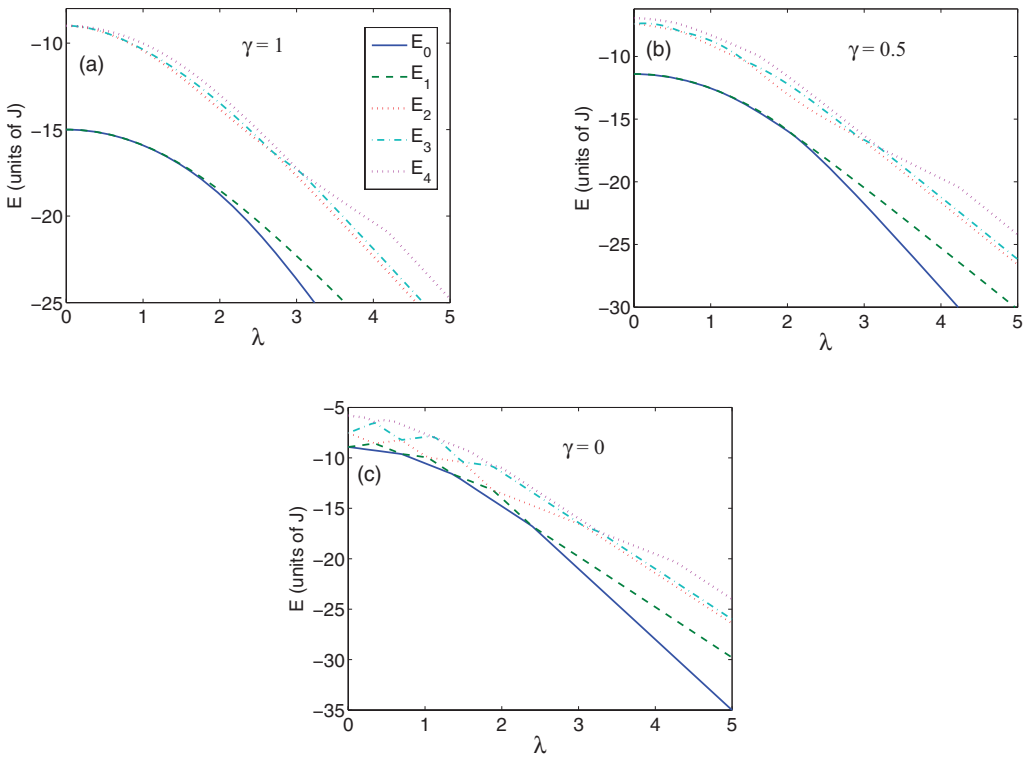

FIG. 6. (Color online) The energy spectrum versus the parameter λ with a single impurity at border site 1 with impurity coupling strength $\alpha = 1$ for different degrees of anisotropy $\gamma = 1,0.5,0$ as shown in the subfigures. The legend for all subfigures is as shown in (a).

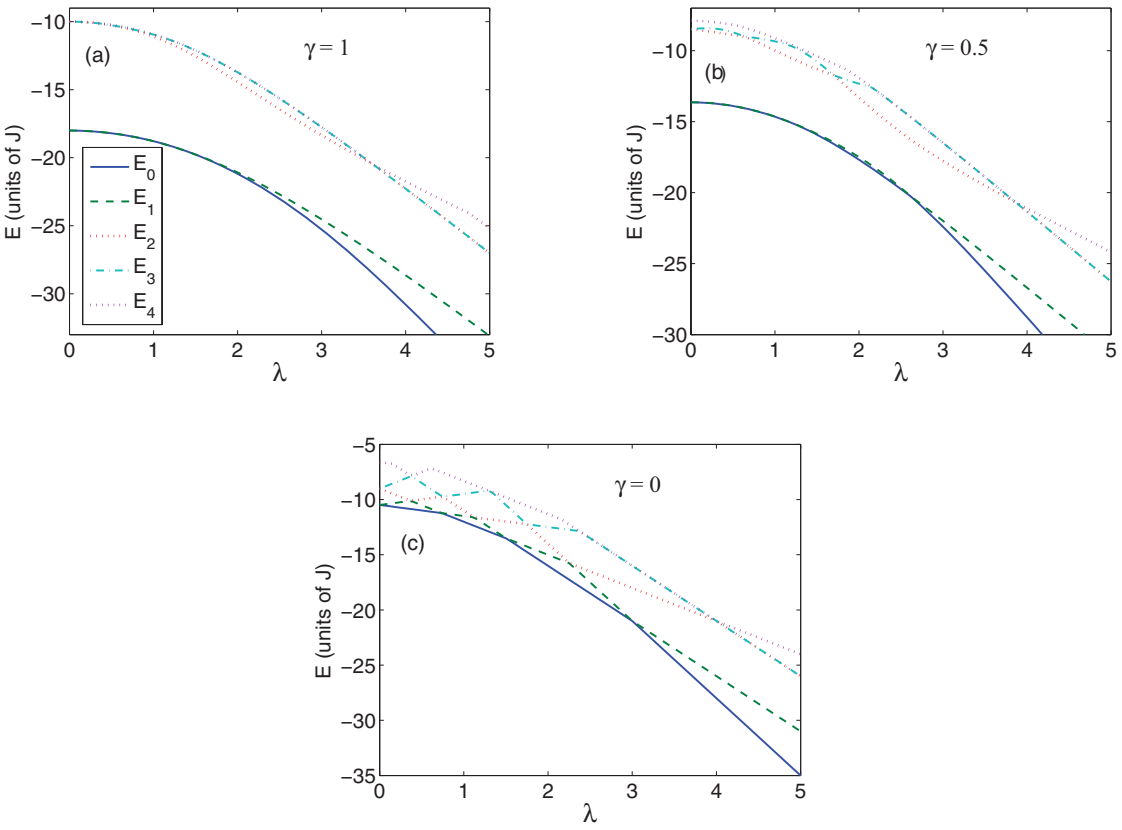

FIG. 7. (Color online) The energy spectrum versus the parameter λ with a single impurity at central site 4 with impurity coupling strength $\alpha = 1$ for different degrees of anisotropy $\gamma = 1,0.5,0$ as shown in the subfigures. The legend for all subfigures is as shown in (a).

distinct behavior of the energy spectrum corresponding to $\gamma = 0$ was the reason for the sharp step behavior of the entanglement as was shown in Figs. 2 and 3. Critical quantum behavior in a many-body system happens either when an actual crossing takes place between the excited state and the ground state or a limiting avoided level crossing between them exists, i.e., an energy gap between the two states that vanishes in the infinite system size limit at the critical point [20]. When a many-body system crosses a critical point, significant changes in both its wave function and ground-state energy take place, which are manifested in the behavior of the entanglement function. The entanglement in one-dimensional infinite spin systems, Ising, and XY, was shown to demonstrate scaling behavior in the vicinity of critical points [23]. The change in the entanglement across the critical point was quantified by considering the derivative of the concurrence with respect to the parameter λ. This derivative was explored versus λ for different system sizes, and although it did not show divergence for finite system sizes, it showed clear anomalies which developed into a singularity at the thermodynamic limit. The ground state of the Heisenberg spin model is known to have a double degeneracy for an odd number of spins, which is never achieved unless the thermodynamic limit is reached [20]. Particularly, the Ising 1D spin chain in an external transverse magnetic field has a doubly degenerate ground state in a ferromagnetic phase that is gapped from the excitation spectrum by $2J(1 - h/J)$, which is removed at the critical point and the system becomes a paramagnetic phase. Now, let us first consider our two-dimensional finite-size Ising spin system. The concurrence C_{14} and its first derivative are depicted versus λ in Figs. 8(a) and 8(b), respectively. As one can see, the derivative of the concurrence shows a strong tendency for being singular at $\lambda_c = 1.64$. The characteristics of the energy gap between the ground state and the first excited state as a function of λ are explored in Fig. 8(c). The system shows strict double degeneracy, zero energy gap, only at $\lambda = 0$, i.e., at zero magnetic field, but once the magnetic field is on, the degeneracy is lifted, and an extremely small energy gap develops, which increases very slowly for small magnetic-field values but increases abruptly at certain λ values. It is important to emphasize here that, at $\lambda = 0$, regardless of which one of the double ground states is selected for evaluating the entanglement, the same value is obtained. The critical point of a phase transition should be characterized by a singularity in the ground-state energy and an abrupt change in the energy gap of the system as a function of the system parameter as it crosses the critical point. To better understand the behavior of the energy gap across the prospective critical point and to identify it, we plot the first and second derivatives of the energy gap as a function of λ in Fig. 8(d). Interestingly, the first derivative $d\,\Delta E/d\lambda$, which represents the rate of change in the energy gap as a function of λ, starts with a zero value at $\lambda = 0$ and then increases very slowly before it shows a great rate of change and finally reaches a saturation value. This behavior is best represented by the second derivative $d^2\Delta E/d\lambda^2$, which shows a strong tendency for being singular at $\lambda_c = 1.8$, which indicates the highest rate of change in the energy gap as a function of λ. The

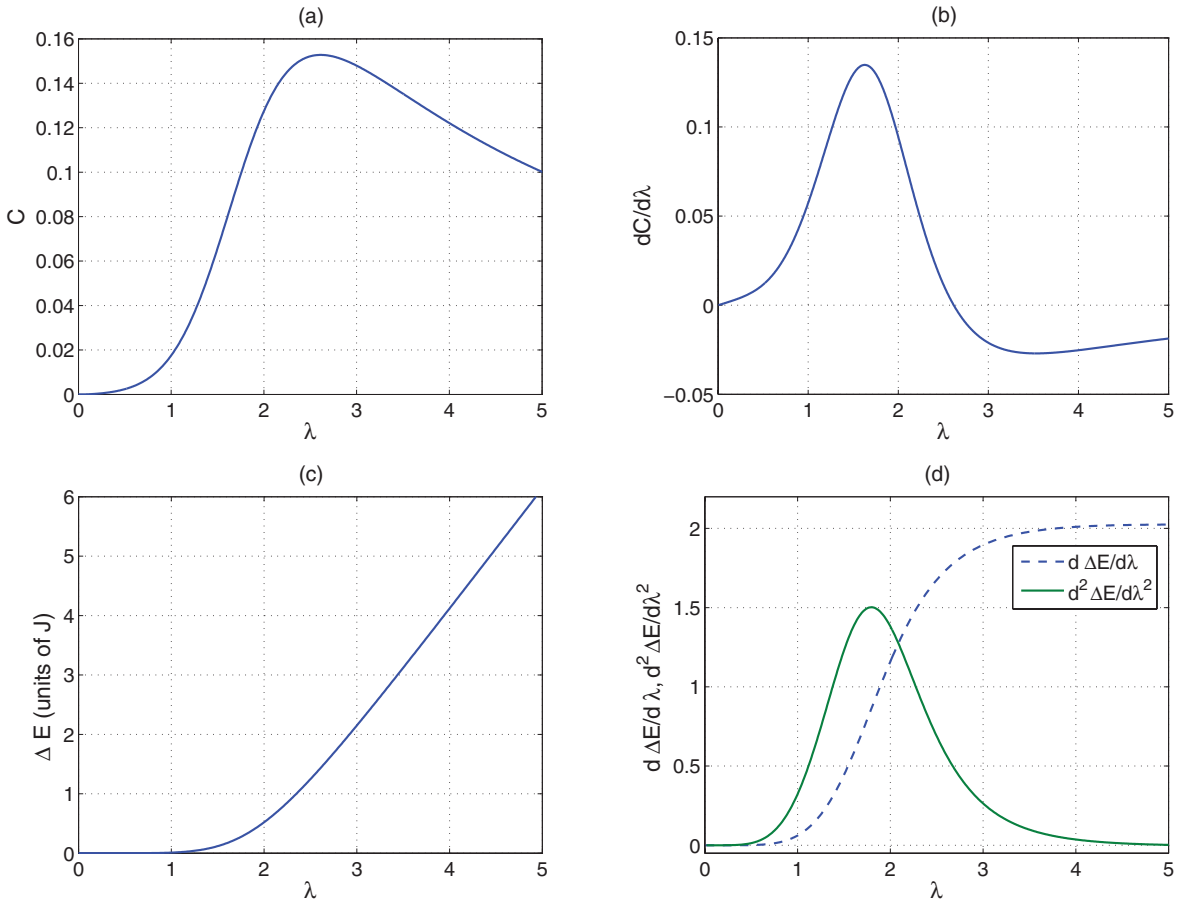

FIG. 8. (Color online) (a) The concurrence C_{14} versus λ, (b) the first derivative of the concurrence C_{14} with respect to λ versus λ, (c) the energy gap between the ground state and the first excited state versus λ, and (d) the first derivative (in units of J) and second derivative (in units of J^2) of the energy gap with respect to λ versus λ for the pure Ising system ($\gamma = 1$ and $\alpha = 0$).

reason for the small discrepancy between the two values of λ_c extracted from the $dC/d\lambda$ plot and the one of $d^2\Delta E/d\lambda^2$ is that the concurrence C_{14} is only between two sites and does not represent the whole system contrary to the energy gap. One can conclude that the rate of change in the energy gap as a function of the system parameter, λ in our case, should be maximum across the critical point. Turning to the case of the partially anisotropic spin system, $\gamma = 0.5$, presented in Fig. 9, one can notice from Fig. 9(a) that the concurrence shows few sharp changes, which is reflected in the energy-gap plot as an equal number of minima as shown in Fig. 9(b). Nevertheless, again, there is only one strict double degeneracy at $\lambda = 0$, whereas, the other three energy-gap minima are nonzero and on the order of 10^{-5}. It is interesting to notice that the anomalies in both $dC/d\lambda$ and $d^2\Delta E/d\lambda^2$ are much stronger and sharper compared with the Ising case as shown in Figs. 9(c) and 9(d). Finally, the isotropic system, which is depicted in Fig. 10, shows even sharper energy gap changes as a result of the sharp changes in the concurrence, and the anomalies in the derivatives $dC/d\lambda$ and $d^2\Delta E/d\lambda^2$ are even much stronger than the previous two cases.

D. System dynamics with impurity

Now, we turn to the dynamics of the two-dimensional spin system under the effect of a single impurity and different degrees of anisotropy. We investigate the dynamical reaction of the system to an applied time-dependent magnetic field with exponential form $h(t) = b + (a - b)e^{-wt}$ for $t > 0$ and $h(t) = a$ for $t \leqslant 0$.

We start by considering the Ising system $\gamma = 1$ with a single impurity at border site 1, which is explored in Fig. 11 where we set $a = 1$, $b = 3.5$, and $\omega = 0.1$. For the pure case $\alpha = 0$, shown in Fig. 11(a), the results confirm the ergodic behavior of the system that was demonstrated in our previous paper [22] where the asymptotic value of the entanglement coincides with the equilibrium state value at $h(t) = b$. As can be noticed from Figs. 11(b)–11(d), neither the weak nor the strong impurities have an effect on the ergodicity of the Ising system. Nevertheless, there is a clear effect on the asymptotic value of entanglements $C(1,2)$ and $C(1,4)$ but not on $C(2,4)$, which relates two regular sites. The weak impurity $\alpha = -0.5$ reduces the asymptotic value of $C(1,2)$ and $C(1,4)$, whereas, the strong impurities $\alpha = 1,2$ raise it compared to the pure case. In Fig. 12, we consider the same system but under the effect of a weaker exponential magnetic field with the set of parameters $a = 1$, $b = 1.5$, and $\omega = 0.1$. As can be noticed, the entanglement of the Ising system is still showing an ergodic behavior at all impurity strengths. This means that the Ising system with a single border impurity is always ergodic under the effect of different impurity strengths and different magnetic-field parameters.

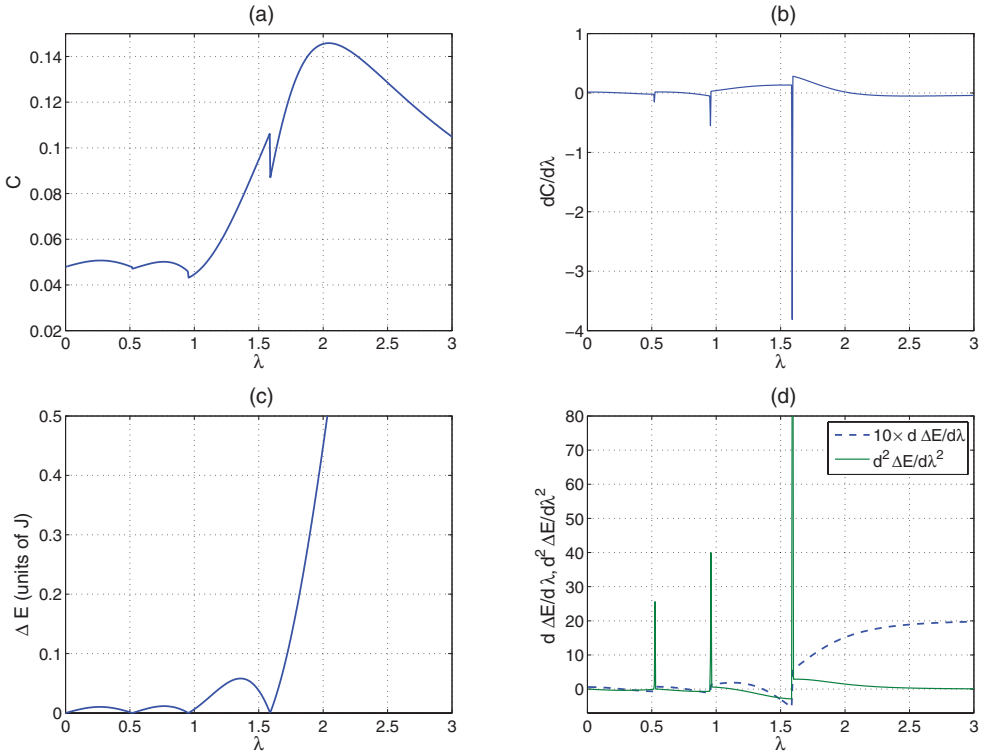

FIG. 9. (Color online) (a) The concurrence C_{14} versus λ, (b) the first derivative of the concurrence C_{14} with respect to λ versus λ, (c) the energy gap between the ground state and the first excited state versus λ, and (d) the first derivative (in units of J) and second derivative (in units of J^2) of the energy gap with respect to λ versus λ for the pure partially anisotropic system ($\gamma = 0.5$ and $\alpha = 0$). Notice that the first derivative of the energy gap is enlarged ten times its actual scale for clearness.

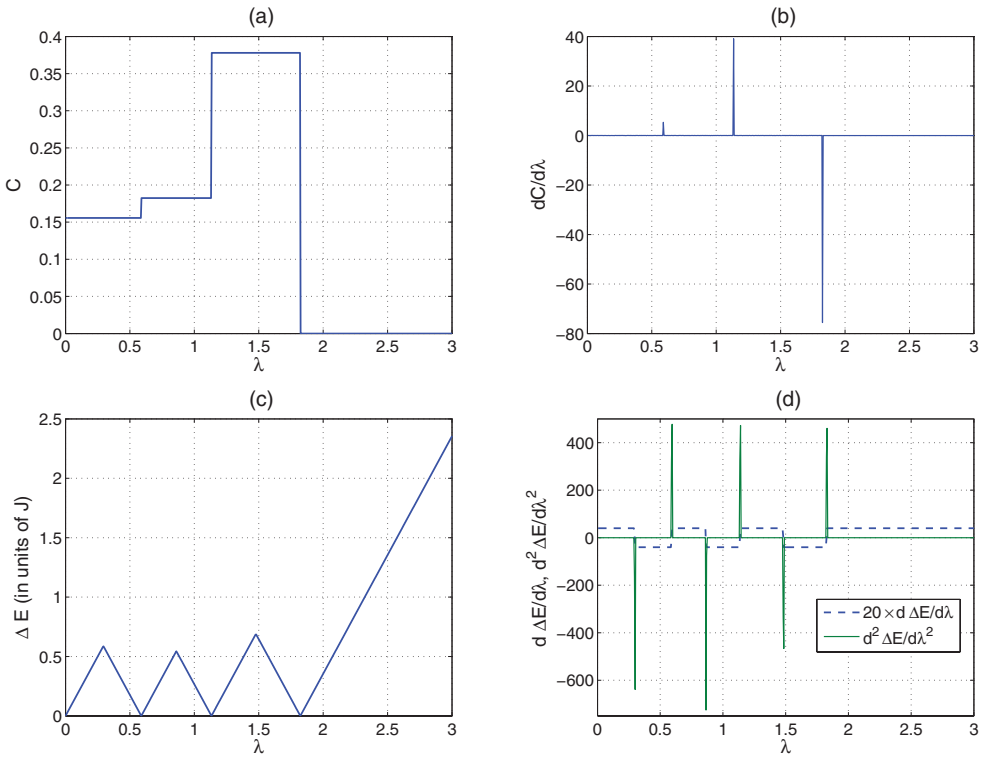

FIG. 10. (Color online) (a) The concurrence C_{14} versus λ, (b) the first derivative of concurrence C_{14} with respect to λ versus λ, (c) the energy gap between the ground state and first excited state versus λ, and (d) the first derivative (in units of J) and second derivative (in units of J^2) of the energy gap with respect to λ versus λ for the pure isotropic system ($\gamma = 0$ and $\alpha = 0$). Notice that the first derivative of the energy gap is enlarged 20 times its actual scale for clearness.

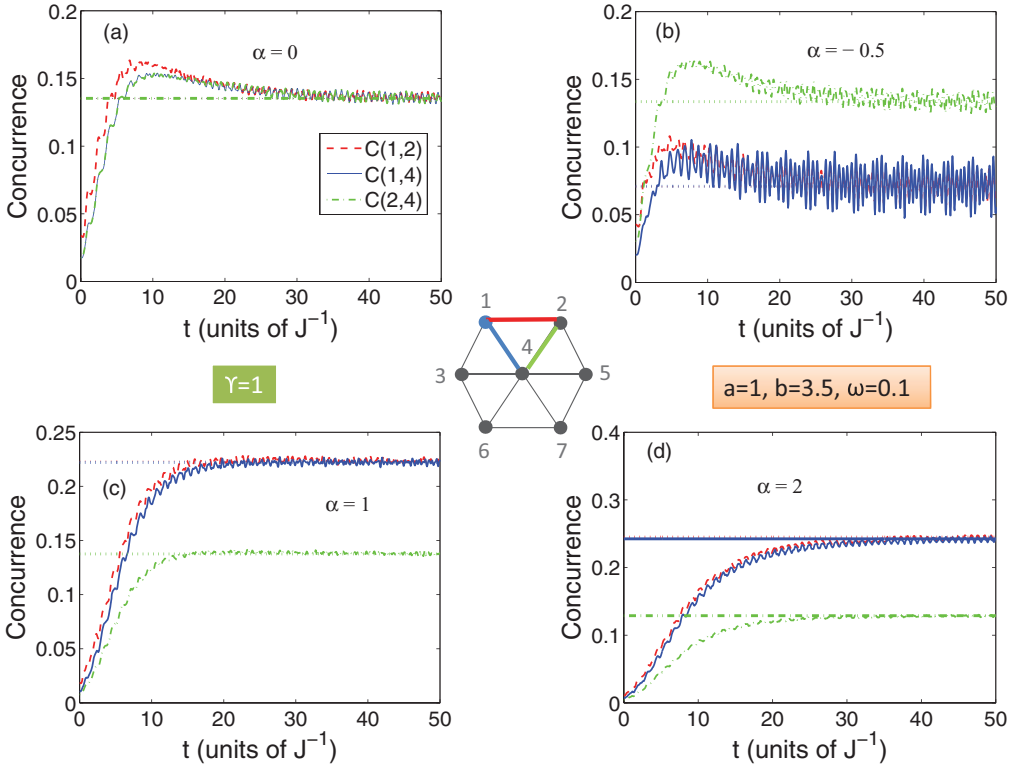

FIG. 11. (Color online) Dynamics of the concurrences $C(1,2), C(1,4), C(2,4)$ with a single impurity at border site 1 with different impurity coupling strengths $\alpha = -0.5, 0, 1, 2$ for the two-dimensional Ising lattice ($\gamma = 1$) under the effect of an exponential magnetic field with parameter values $a = 1$, $b = 3.5$, and $\omega = 0.1$. The straight lines represent the equilibrium concurrences corresponding to constant magnetic field $h = 3.5$. The legend for all subfigures is as shown in (a).

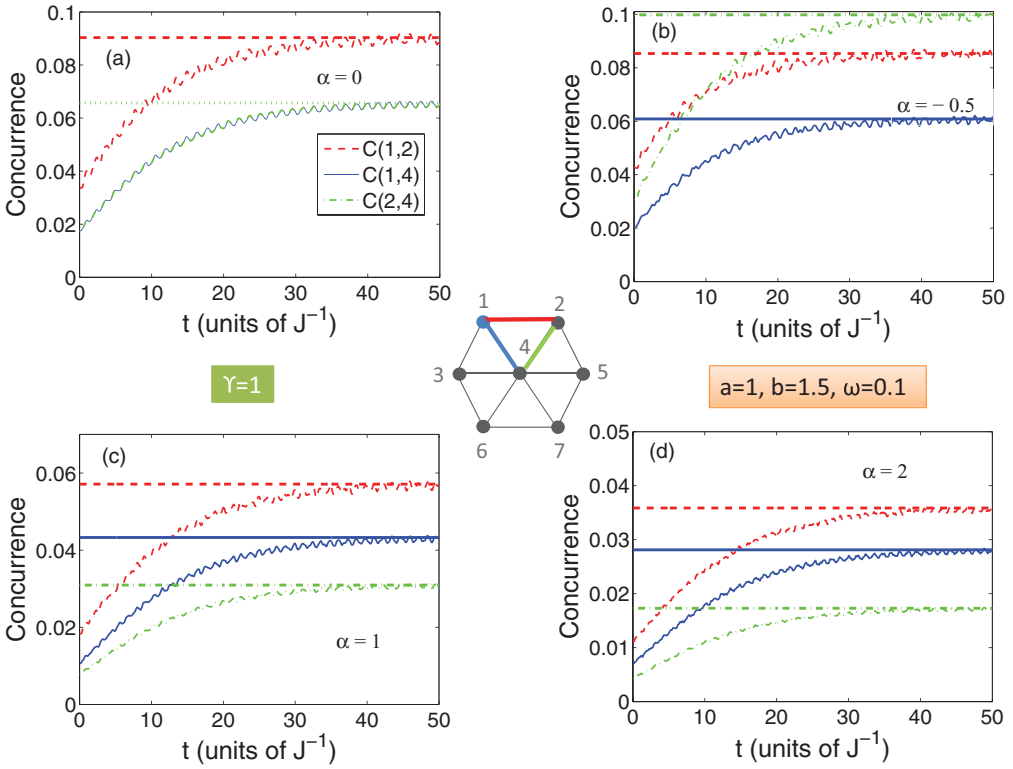

FIG. 12. (Color online) Dynamics of the concurrences $C(1,2), C(1,4), C(2,4)$ with a single impurity at border site 1 with different impurity coupling strengths $\alpha = -0.5, 0, 1, 2$ for the two-dimensional Ising lattice ($\gamma = 1$) under the effect of an exponential magnetic field with parameter values $a = 1$, $b = 1.5$, and $\omega = 0.1$. The straight lines represent the equilibrium concurrences corresponding to constant magnetic field $h = 1.5$. The legend for all subfigures is as shown in (a).

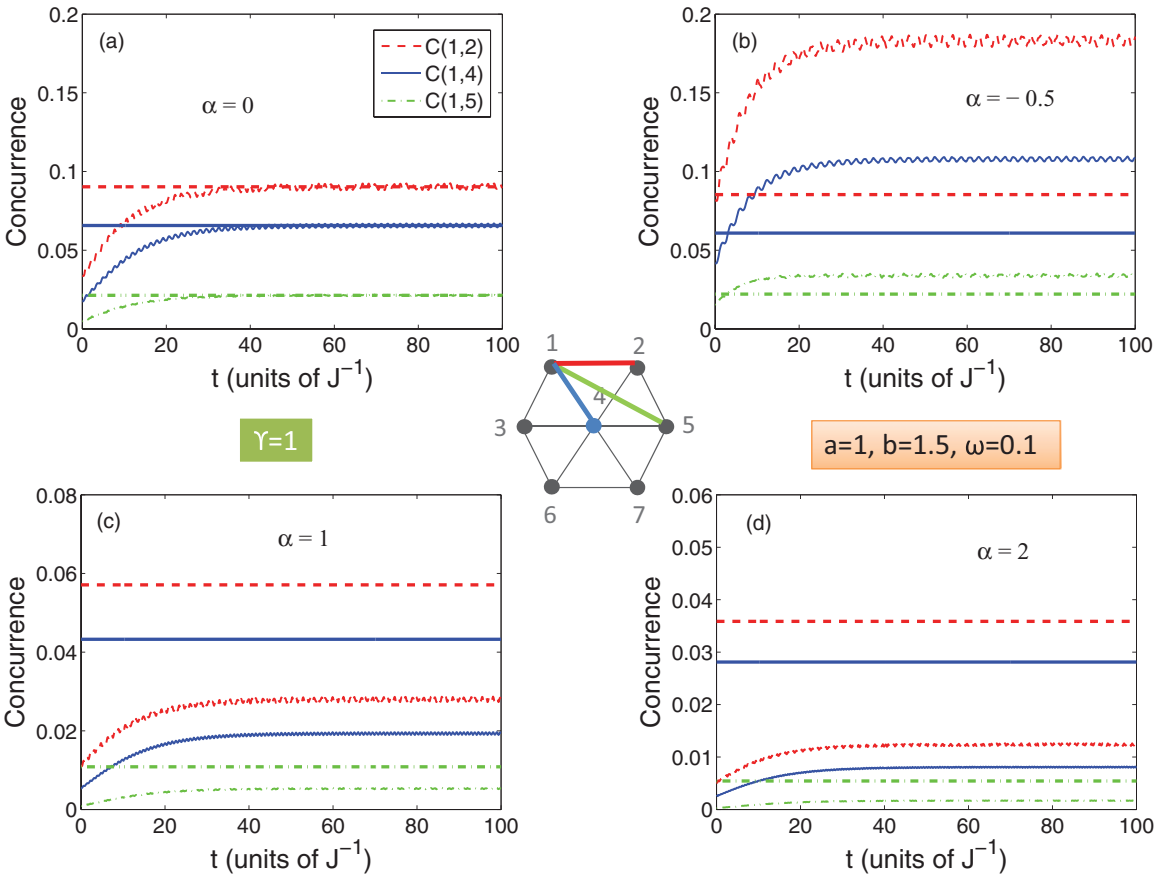

FIG. 13. (Color online) Dynamics of the concurrences $C(1,2), C(1,4), C(1,5)$ with a single impurity at central site 4 with different impurity coupling strengths $\alpha = -0.5, 0, 1, 2$ for the two-dimensional Ising lattice ($\gamma = 1$) under the effect of an exponential magnetic field with parameter values $a = 1$, $b = 1.5$, and $\omega = 0.1$. The straight lines represent the equilibrium concurrences corresponding to constant magnetic field $h = 1.5$. The legend for all subfigures is as shown in (a).

Interestingly, the different impurity strengths have different effects on the asymptotic value of the entanglements compared to the previous case under the effect of the new magnetic field. The weak impurity, as shown in Fig. 12(b), raises the asymptotic value of $C(2,4)$ and splits those of $C(1,2)$ and $C(1,4)$ from each other. On the other hand, the strong impurity effects are depicted in Figs. 12(c) and 12(d), which show that the asymptotic values of all concurrences are reduced significantly as the impurity strength increases, contrary to the previous case. This emphasis is on the important role that the magnetic-field parameters play beside the impurity strength in controlling the entanglement behavior.

It is of great interest to examine the effect of the impurity location, which we investigate in Fig. 13 where a single impurity is located at central site 4 instead of border site 1 with exponential magnetic-field parameters $a = 1$, $b = 1.5$, and $\omega = 0.1$. Very interestingly, the entanglement behavior changes significantly as a result of changing the impurity location. Although the pure Ising system is still ergodic as shown in Fig. 13(a), the system with weak and strong impurities becomes nonergodic, which is illustrated in Figs. 13(b)–13(d), respectively. Again, the weak impurity raises the asymptotic values, whereas, the strong impurities reduce them significantly. The dynamics of the partially anisotropic XY system, under the effect of the exponential magnetic field with parameters $a = 1$, $b = 3.5$, and $\omega = 0.1$, is explored in Fig. 14. It is remarkable to see that, while for both the pure and the weak impurity cases $\alpha = 0$ and -0.5, the system is nonergodic as shown in Figs. 14(a) and 14(b), and it is ergodic in the strong impurity cases $\alpha = 1$ and 2 as illustrated in Figs. 14(c) and 14(d). Clearly, the asymptotic values of the entanglement are higher in the pure and weak impurity cases compared with the strong impurities. Changing the magnetic-field parameter value b to 1.5, one can observe the great impact in Fig. 15 where only the pure system becomes ergodic, whereas, the system with any impurity strength is nonergodic. This means that the magnetic-field parameters control ergodicity as well. In Fig. 16, we study the same system with a single impurity at central site 4 with magnetic-field parameters $a = 1$, $b = 1.5$, and $\omega = 0.1$. As can be seen from the different subfigures, the system is ergodic only in the pure case, and the asymptotic values are higher for the pure and weak impurity systems compared with the strong impurities. The complete isotropic XY system with a single border impurity at site 1 under the effect of an exponential magnetic field with parameter values $a = 1$, $b = 1.5$, and $\omega = 0.1$ is investigated in Fig. 17. The trivial effect of the magnetic field, similar to the one-dimensional case results [8], is clear where the entanglement assumes a constant value for all pair of spins.

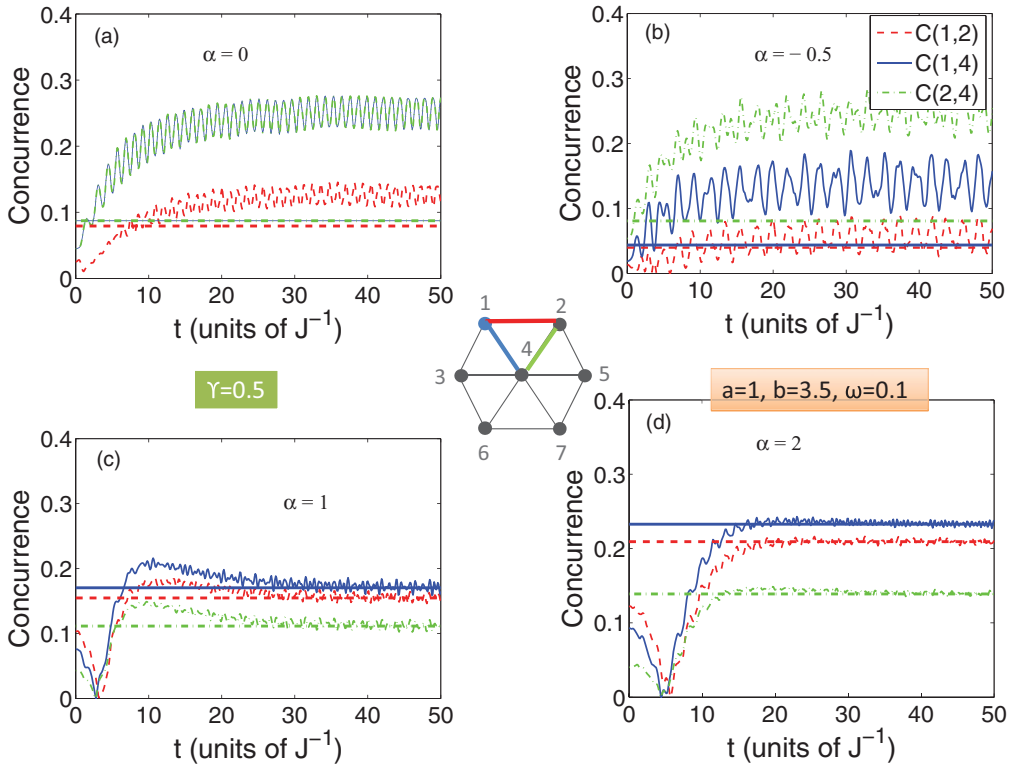

FIG. 14. (Color online) Dynamics of the concurrences $C(1,2), C(1,4), C(2,4)$ with a single impurity at border site 1 with different impurity coupling strengths $\alpha = -0.5, 0, 1, 2$ for the two-dimensional partially anisotropic lattice ($\gamma = 0.5$) under the effect of an exponential magnetic field with parameter values $a = 1$, $b = 1.5$, and $\omega = 0.1$. The straight lines represent the equilibrium concurrences corresponding to constant magnetic field $h = 3.5$. The legend for all subfigures is as shown in (b).

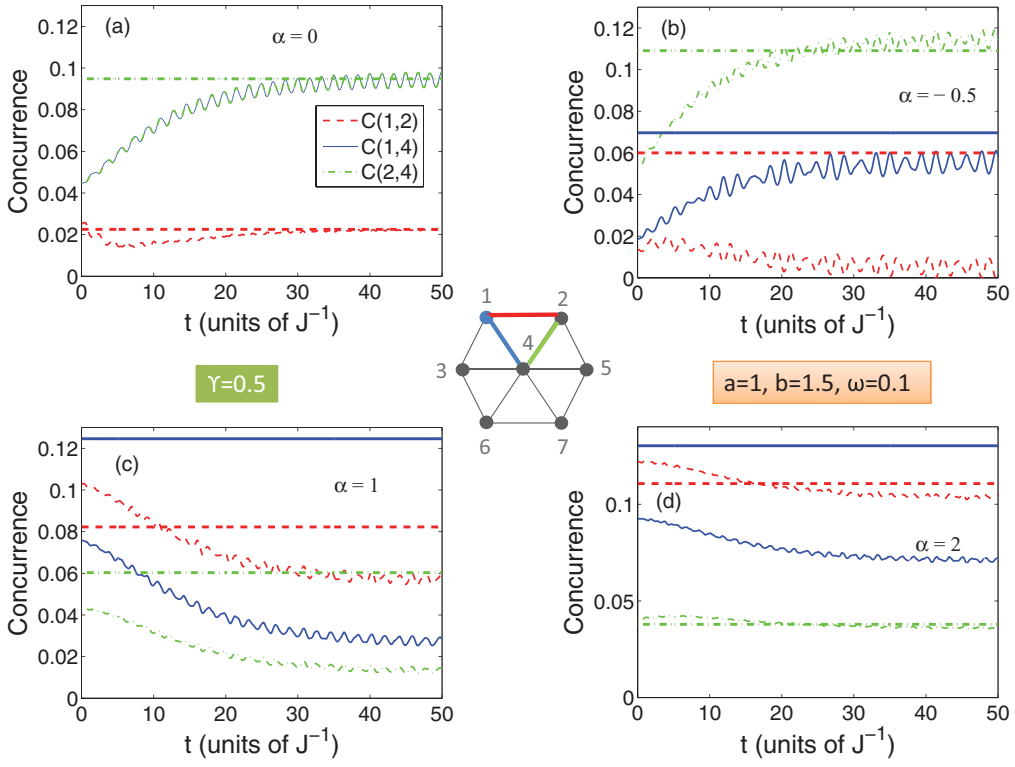

FIG. 15. (Color online) Dynamics of the concurrences $C(1,2), C(1,4), C(2,4)$ with a single impurity at border site 1 with different impurity coupling strengths $\alpha = -0.5, 0, 1, 2$ for the two-dimensional partially anisotropic lattice ($\gamma = 0.5$) under the effect of an exponential magnetic field with parameter values $a = 1$, $b = 1.5$, and $\omega = 0.1$. The straight lines represent the equilibrium concurrences corresponding to constant magnetic field $h = 1.5$. The legend for all subfigures is as shown in (a).

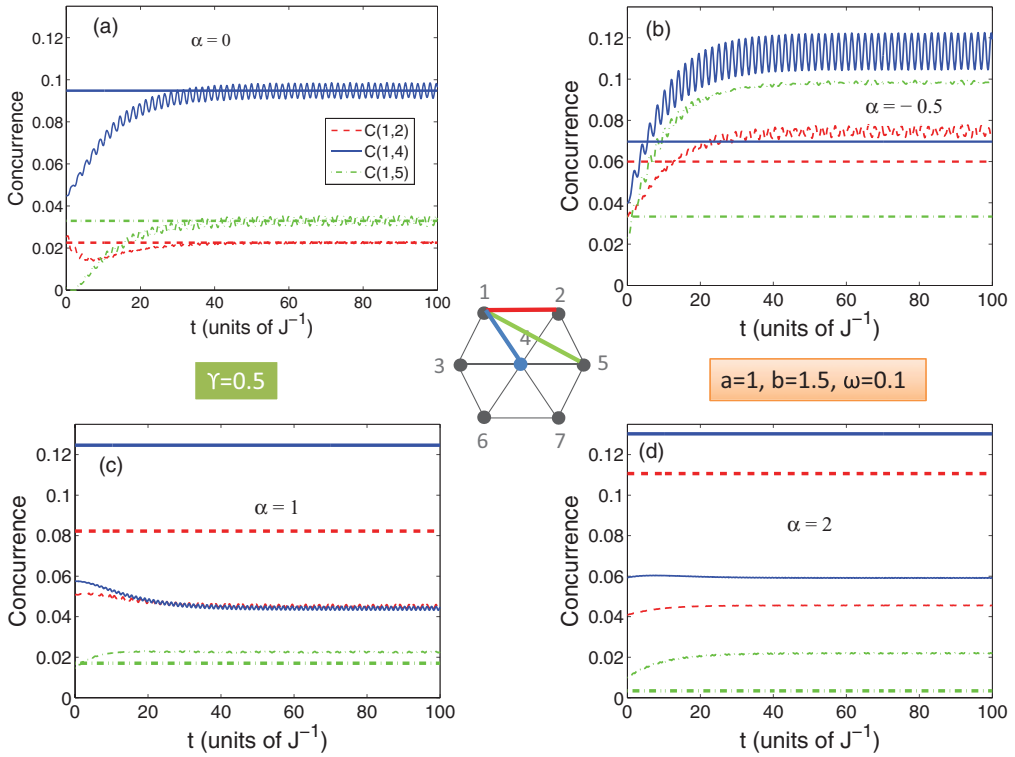

FIG. 16. (Color online) Dynamics of the concurrences $C(1,2), C(1,4), C(2,4)$ with a single impurity at central site 4 with different impurity coupling strengths $\alpha = -0.5, 0, 1, 2$ for the two-dimensional partially anisotropic lattice ($\gamma = 0.5$) under the effect of an exponential magnetic field with parameter values $a = 1$, $b = 1.5$, and $\omega = 0.1$. The straight lines represent the equilibrium concurrences corresponding to constant magnetic field $h = 1.5$. The legend for all subfigures is as shown in (a).

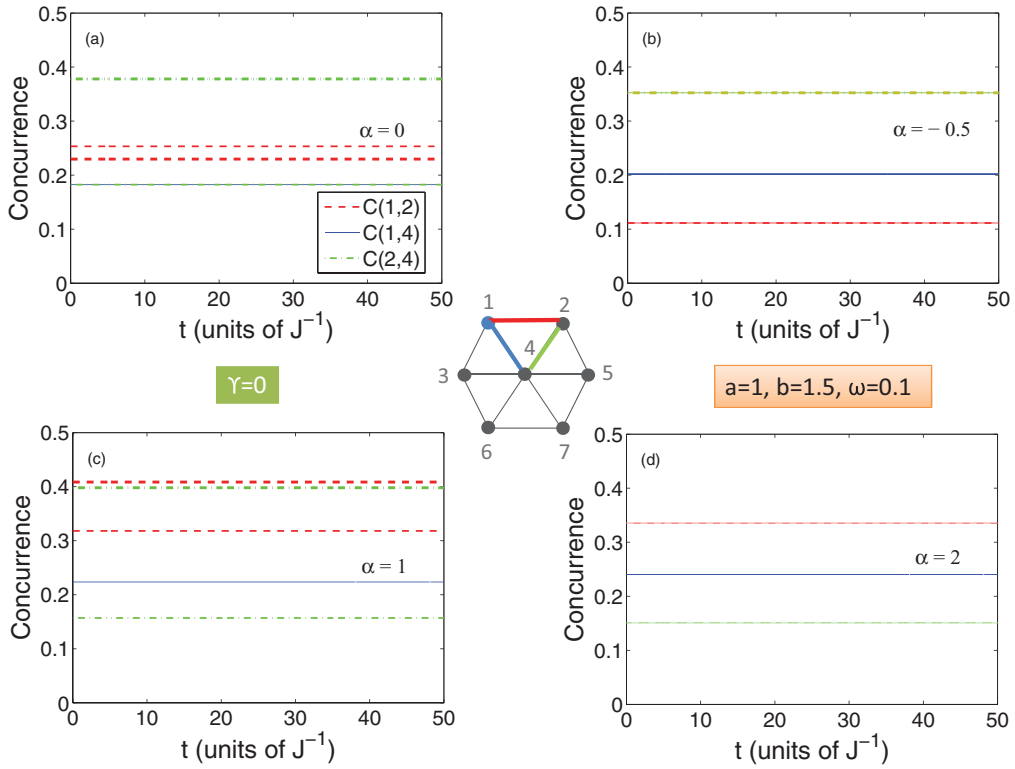

FIG. 17. (Color online) Dynamics of the concurrences $C(1,2), C(1,4), C(2,4)$ with a single impurity at border site 1 with different impurity coupling strengths $\alpha = -0.5, 0, 1, 2$ for the two-dimensional XY lattice ($\gamma = 0$) under the effect of an exponential magnetic field with parameter values $a = 1$, $b = 1.5$, and $\omega = 0.1$. The straight (thicker) lines represent the equilibrium concurrences corresponding to constant magnetic field $h = 1.5$. The legend for all subfigures is as shown in (a).

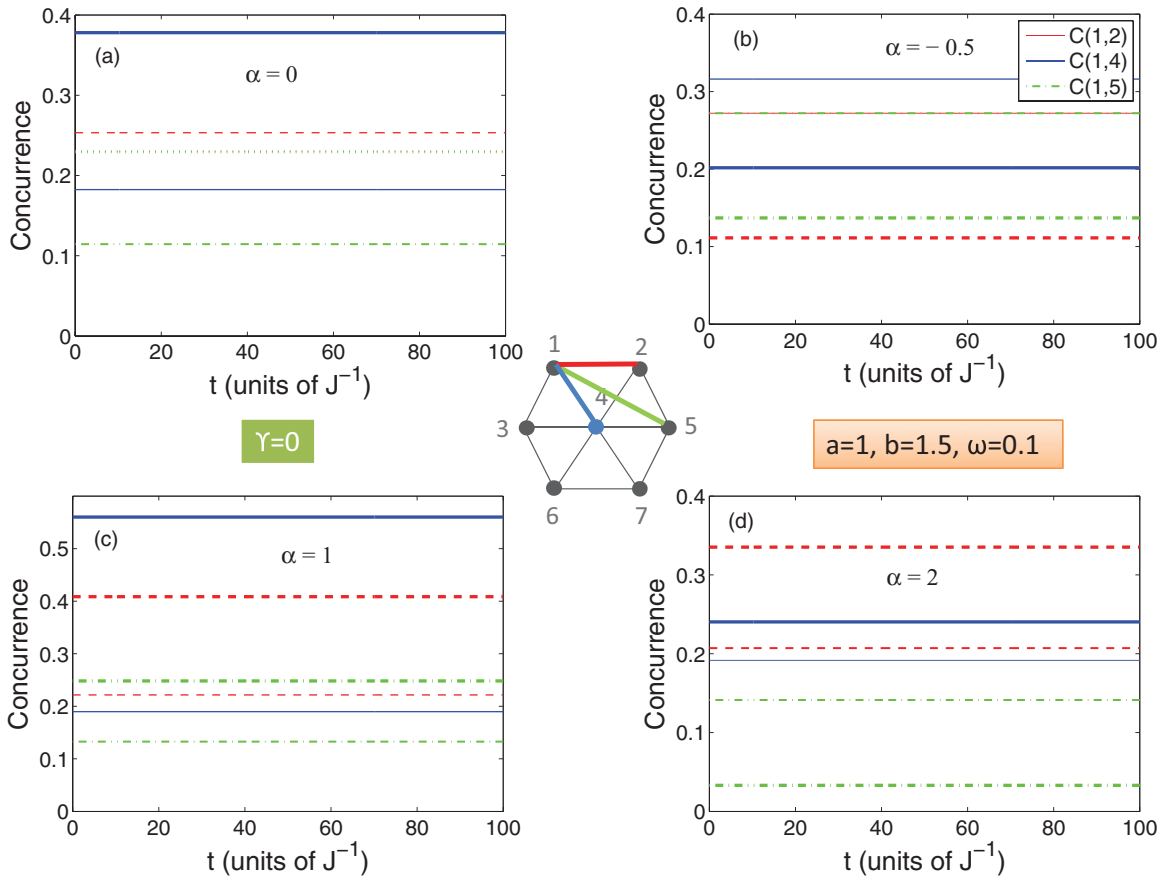

FIG. 18. (Color online) Dynamics of the concurrences $C(1,2), C(1,4), C(2,4)$ with a single impurity at central site 4 with different impurity coupling strengths $\alpha = -0.5, 0, 1, 2$ for the two-dimensional XY lattice ($\gamma = 0$) under the effect of an exponential magnetic field with parameter values $a = 1$, $b = 1.5$, and $\omega = 0.1$. The straight (thicker) lines represent the equilibrium concurrences corresponding to constant magnetic field $h = 1.5$. The legend for all subfigures is as shown in (b).

This trivial effect is the result of the fact that, for $\gamma = 0$, the exchange-coupling terms in the Hamiltonian commute with the magnetic-field term. Nevertheless, one still can see an effect of the impurity on the ergodicity of the system where, for $\alpha = 0$ and 1, the system is nonergodic, whereas, for $\alpha = -0.5$ and 2, it is ergodic as shown in Fig. 17. In fact, testing a wide range of α values indicates that, for the values approximately in the range of $-0.4 \geqslant \alpha \leqslant 1.9$, the system is nonergodic, otherwise, it is ergodic, i.e., for small absolute values of the impurity. Examining the same system under the effect of the same magnetic field but with a single central impurity, for a wide range of α, demonstrates that the system becomes nonergodic at all values of α, which is illustrated in Fig. 18.

IV. DOUBLE IMPURITIES

A. Static system with impurities

In this section, we study the effect of double impurity where we start with two located at border sites 1 and 2. We set the coupling strength between the two impurities as $J' = (1 + \alpha_1)J$ between any one of the impurities and its regular nearest neighbors as $J'' = (1 + \alpha_2)J$ and between the rest of the nearest-neighbor sites on the lattice as J. The effect of the impurities' strength on the concurrence between different pairs of sites for the Ising lattice is shown in Fig. 19.

In Fig. 19(a), we consider the entanglement between two impurity sites 1 and 2 under a constant external magnetic field $h = 2$. The concurrence $C(1,2)$ takes a large value when the impurity strengths α_1, controlling the coupling between the impurity sites, is large and when α_2, controlling coupling between impurities and their nearest neighbors, is weak. As α_1 decreases and α_2 increases, $C(1,2)$ decreases monotonically until it vanishes. As one can conclude, α_1 is more effective than α_2 in controlling the entanglement in this case. On the other hand, the entanglement between impurity site 1 and regular central site 4 is illustrated in Fig. 19(b), which behaves completely different from $C(1,2)$. The concurrence $C(1,4)$ is mainly controlled by the impurity strength α_2 where it starts with a very small value when the impurity is very weak and increases monotonically until it reaches a maximum value at $\alpha_2 = 0$, i.e., with no impurity, and decays again as the impurity strength increases. The effect of α_1 in that case is less significant and makes the concurrence slowly decrease as α_1 increases, which is expected since, as the coupling between two border sites 1 and 2 increases, the entanglement between 1 and 4 decreases. It is important to note that, in general, $C(1,2)$ is much larger than $C(1,4)$ since the border entanglement is always higher than the central one as the entanglement is shared by many sites. The entanglement between two regular sites is shown in Fig. 19(c) where the concurrence

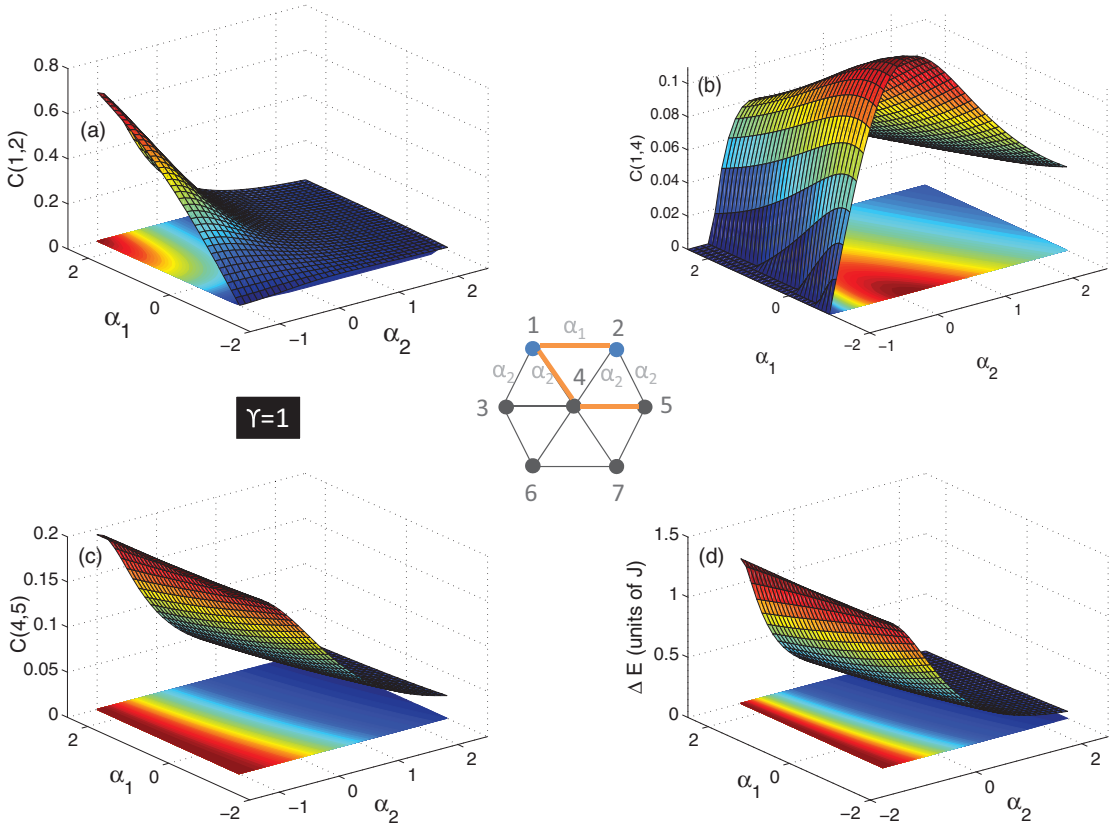

FIG. 19. (Color online) The concurrences $C(1,2), C(1,4), C(4,5)$ versus the impurity coupling strengths α_1 and α_2 with double impurities at sites 1 and 2 for the two-dimensional Ising lattice ($\gamma = 1$) in an external magnetic field $h = 2$.

$C(4,5)$ is depicted against α_1 and α_2, and the entanglement decays gradually as α_2 increases, whereas, α_1 has a very small effect on the entanglement, which slightly decreases as α_1 increases as shown. Interestingly, the behavior of the energy gap between the ground state and the first excited state of the Ising system ΔE versus the impurity strengths α_1 and α_2, which is explored in Fig. 19(d) has a strong resemblance to that of the concurrence $C(4,5)$ except that the decay of ΔE against α_2 is more rapid. The effect of changing the location of the impurities is considered in Fig. 20 where the two impurities exist at sites 1 and 4 in the Ising system. The behavior of the concurrences is very much the same as in the previous case except that the profiles of $C(1,2)$ and $C(1,4)$ have been exchanged as $C(1,4)$ now represents the concurrence between the two impurity sites.

The partially anisotropic system $\gamma = 0.5$ with double impurity at sites 1 and 2 and under the effect of the external magnetic field $h = 2$ is explored in Fig. 21. As one can see, the overall behavior, especially at the border values of the impurity strengths, is the same as observed in the Ising case except that the concurrences suffer a local minimum within a small range of the impurity strength α_2 between 0 and 1 while corresponding to the whole α_1 range. The change in the entanglement around this local minimum takes a steplike profile, which is very clear in the case of the concurrence $C(1,4)$ shown in Fig. 21(b). Remarkably, the local minima in the plotted concurrences coincide with the line of vanishing energy gap as shown in Fig. 21(d), which means that these minima correspond to a transition between a ground state and another one, which takes place as the system parameters change. The anisotropic XY model with two impurities at sites 1 and 2 in an external magnetic field $h = 1.8$ is explored in Fig. 22. The entanglement for this system shows much sharper changes as a function of the impurity strengths and the sharp step changes take place in a narrow region of both α_1 and α_2 specifically for $-1 \leqslant \alpha_1 \leqslant 1$ and $-1 \leqslant \alpha_2 \leqslant 0$. It is interesting to note that, again, the sharp step changes in the entanglement are corresponding to the line of minimum energy gap as shown in Fig. 22(d) where this line varies continuously between a very small value and zero, which explains the many steps appearing in the different concurrences and, particularly, $C(1,4)$ depicted in Fig. 22(b).

B. System dynamics with impurities

Now, we turn to the dynamics of the two-dimensional spin system with double impurity under the effect of an external exponential magnetic field to test the ergodicity of the system as we vary the degree of anisotropy or the location of the impurities. In Fig. 23, we consider the dynamics of the Ising system with two impurities at sites 1 and 2 under the effect of an exponential magnetic field with parameters $a = 1$, $b = 2$, and $\omega = 0.1$. As one can see, the system shows an ergodic behavior for the different values of the impurity strengths $\alpha_1, \alpha_2 = (0,0), (0,1), (1,0)$, and $(1,1)$. The Ising system sustains

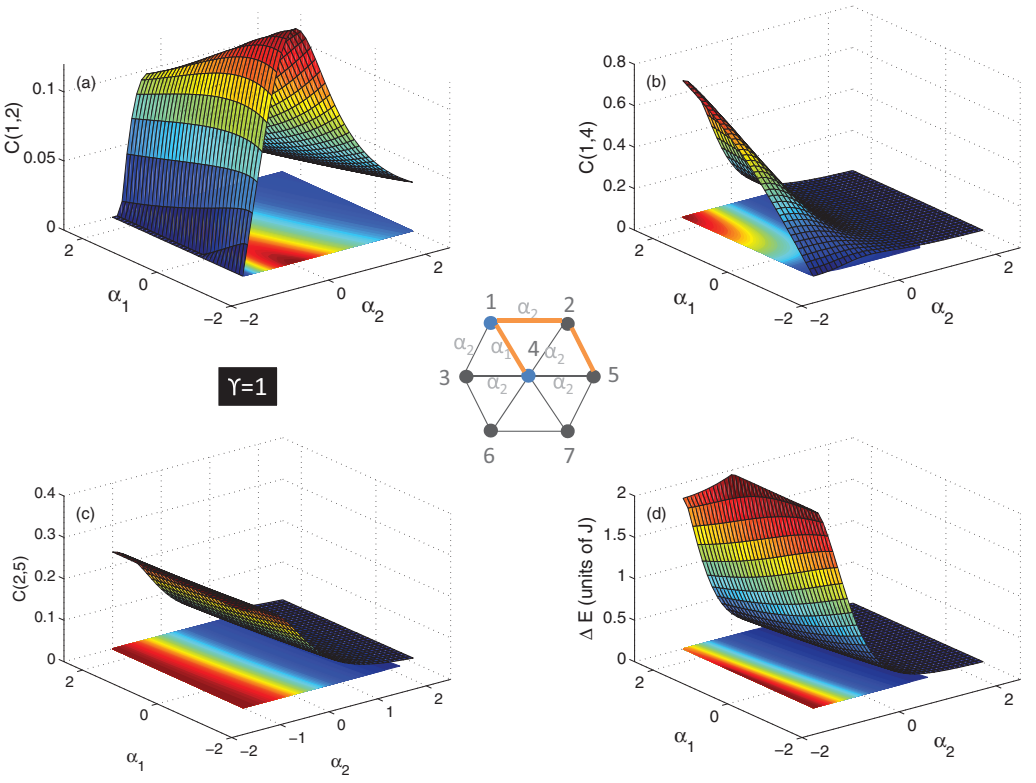

FIG. 20. (Color online) The concurrences $C(1,2), C(1,4), C(2,5)$ and the energy gap ΔE versus the impurity coupling strengths α_1 and α_2 with double impurities at sites 1 and 4 for the two-dimensional Ising lattice ($\gamma = 1$) in an external magnetic field $h = 2$.

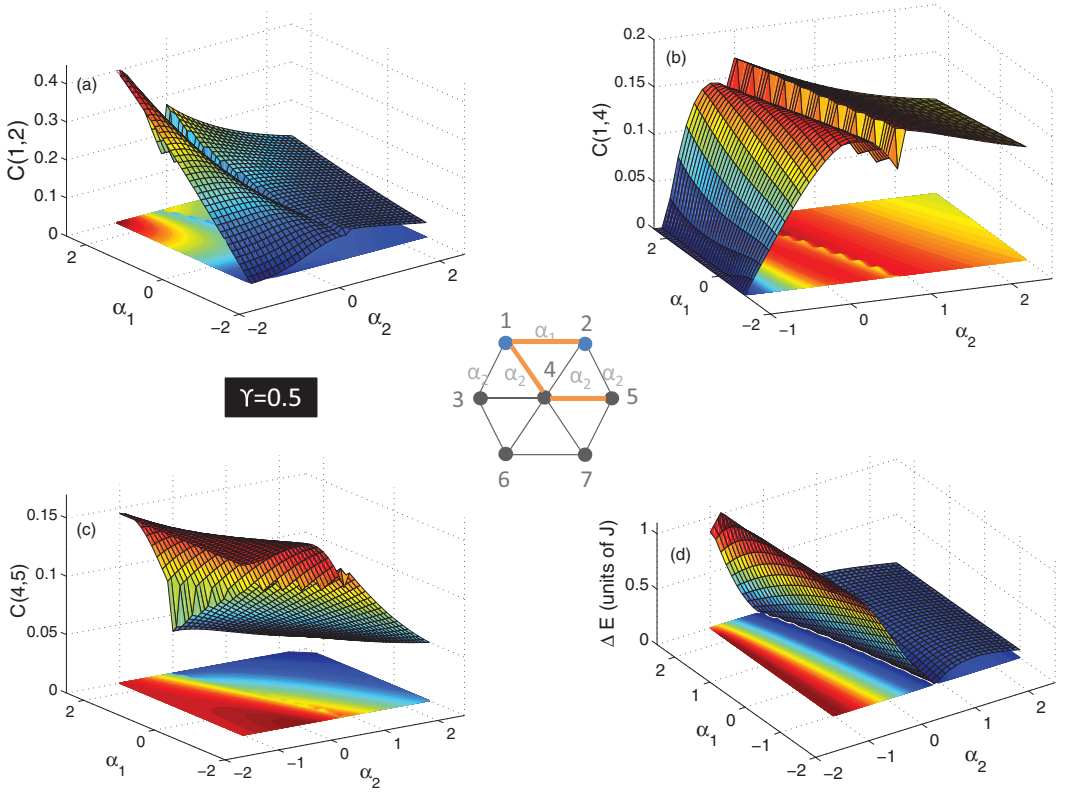

FIG. 21. (Color online) The concurrences $C(1,2), C(1,4), C(4,5)$ versus the impurity coupling strengths α_1 and α_2 with double impurities at sites 1 and 2 for the two-dimensional partially anisotropic lattice ($\gamma = 0.5$) in an external magnetic field $h = 2$.

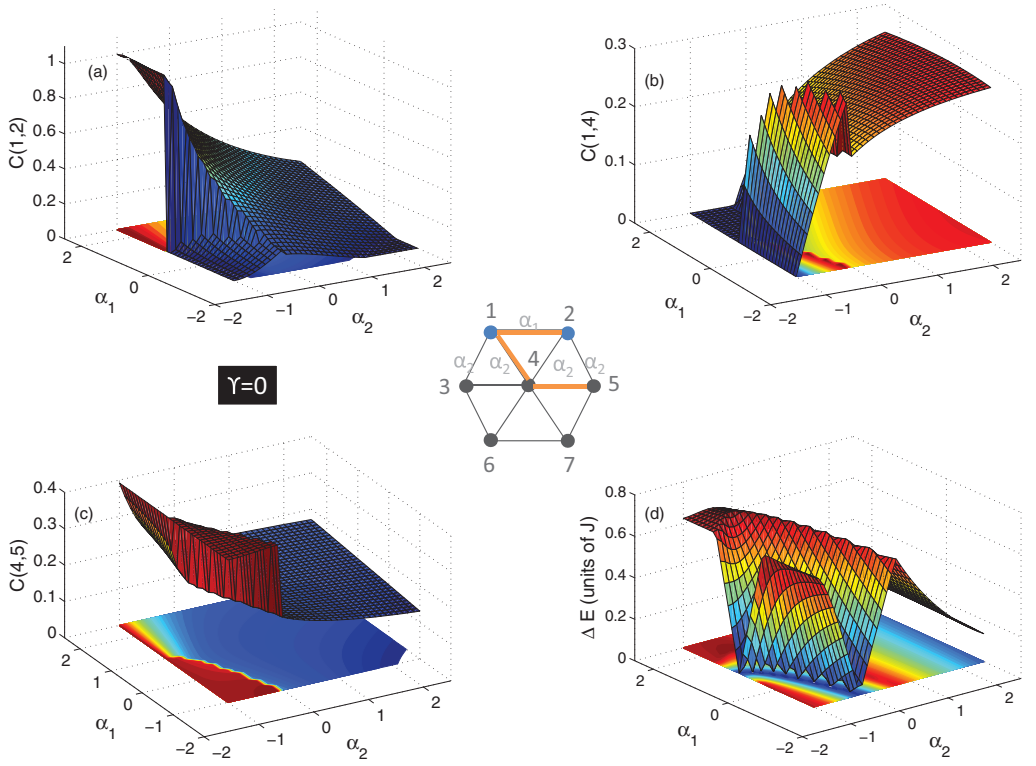

FIG. 22. (Color online) The concurrences $C(1,2), C(1,4), C(4,5)$ versus the impurity coupling strengths α_1 and α_2 with double impurities at sites 1 and 2 for the two-dimensional XY lattice ($\gamma = 0$) in an external magnetic field $h = 2$.

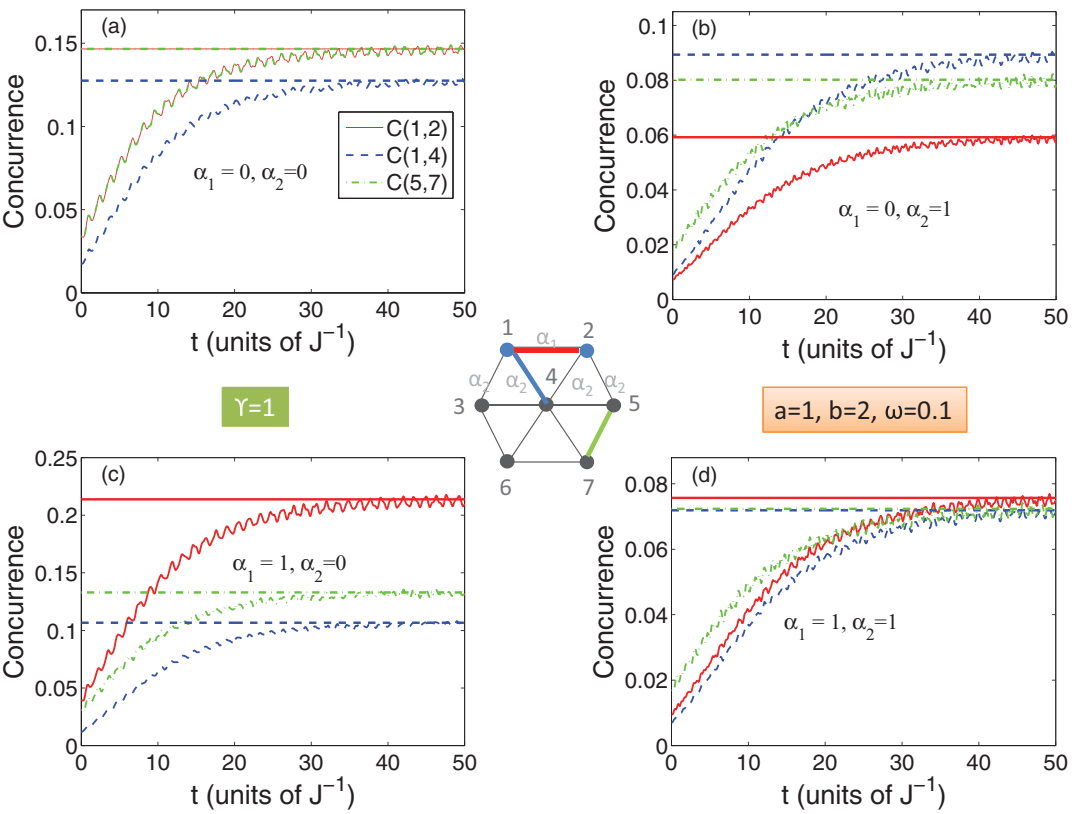

FIG. 23. (Color online) Dynamics of the concurrences $C(1,2), C(1,4), C(5,7)$ with double impurities at sites 1 and 2 for the two-dimensional Ising lattice ($\gamma = 1$) in an exponential magnetic field where $a = 1$, $b = 2$, and $w = 0.1$. The straight lines represent the equilibrium concurrences corresponding to constant magnetic field $h = 2$. The legend for all subfigures is as shown in (a).

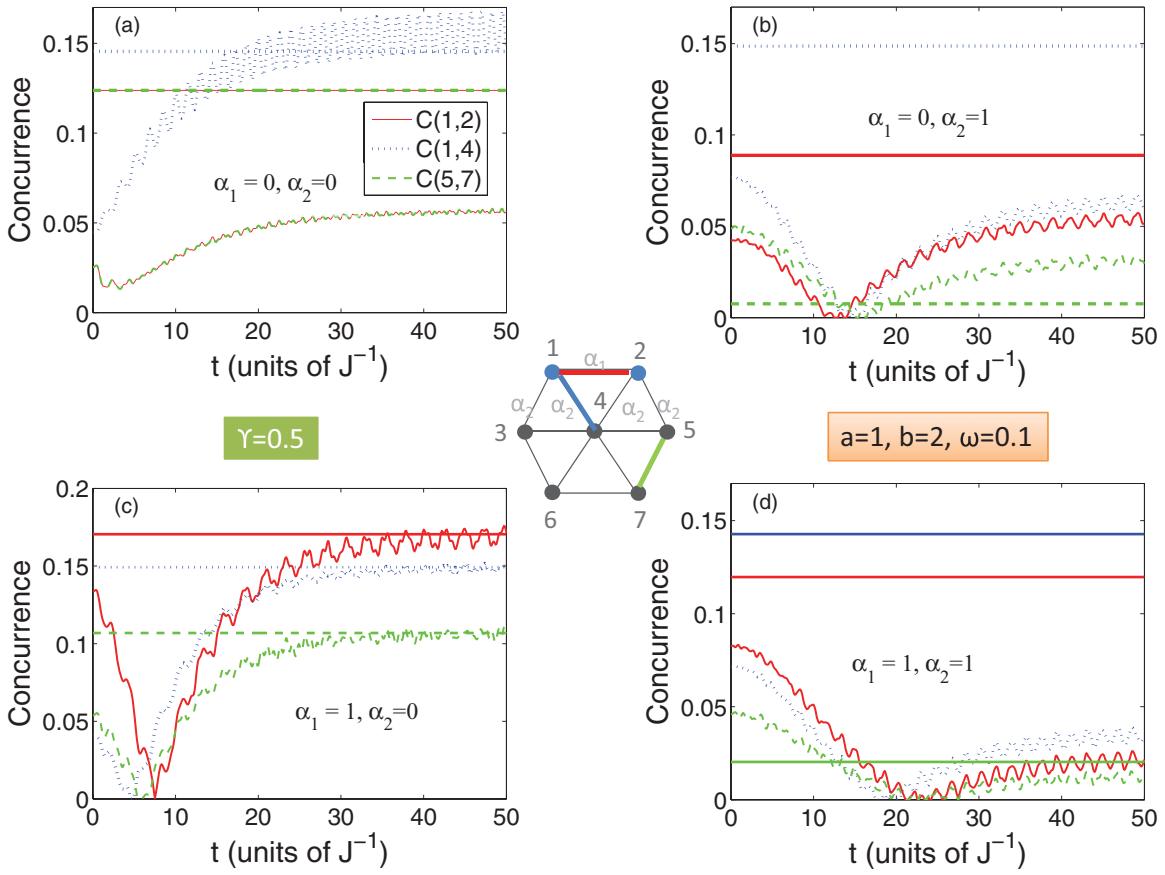

FIG. 24. (Color online) Dynamics of the concurrences $C(1,2), C(1,4), C(5,7)$ with double impurities at sites 1 and 2 for the two-dimensional partially anisotropic lattice ($\gamma = 0.5$) in an exponential magnetic field where $a = 1$, $b = 2$, and $w = 0.1$. The straight lines represent the equilibrium concurrences corresponding to constant magnetic field $h = 2$. The legend for all subfigures is as shown in (a).

its ergodicity for all shown values of impurities strengths and other tested values. The partially anisotropic system, under the same condition, behaves differently. Its pure case, the $\alpha_1,\alpha_2 = (0,1)$ case, and the $\alpha_1, \alpha_2 = (1,1)$ case are all nonergodic as depicted in Figs. 24(a) and 24(b). Nevertheless, the system with impurity strengths $\alpha_1 = 1$ and $\alpha_2 = 0$ shows ergodic behavior, which means that the nonergodicity of the partially anisotropic system is sensitive for the strength and location of the impurities. The isotropic system is explored in Fig. 25, which behaves nonergodically for all impurity strengths. Testing the effect of the impurity location, we consider the same system with impurities at sites 1 and 4 (see Fig. 26). Whereas, the Ising system shows ergodicity at all impurity strengths as shown in Fig. 23, the partially and isotropic XY systems are nonergodic at the different impurity strengths as plotted in Figs. 27 and 28, respectively.

V. CONCLUSION AND FUTURE DIRECTIONS

We have investigated the nearest-neighbor entanglement and ergodicity of a two-dimensional XY spin lattice in an external magnetic field h. The spins are coupled to each other through nearest-neighbor exchange interaction J. The number of spins in the lattice is 7 where we may consider one or two of them as impurities. We have found that the completely anisotropic (the Ising), the partially anisotropic, and the isotropic systems behave in a very similar fashion to that of the one-dimensional spin systems at the extreme, small, and large values of the parameter $\lambda = h/J$ but may deviate at the intermediate values. The first two systems show phase transition in the vicinity of the parameter critical value $\lambda = 2$, and their entanglement vanishes as λ increases. The entanglement of the isotropic system changes in a sharp step profile before suddenly vanishing in the vicinity of $\lambda = 2$. The entanglement dynamics of the system with impurities was investigated under the effect of an external time-dependent magnetic field of exponential form. It was found that the ergodicity of the system can be tuned using the strength and location of the impurities as well as the degree of anisotropy of the coupling between the spins. In the future, it would be interesting to investigate the same systems coupled to a dissipative environment and to examine the effect of impurity to tune the decoherence in the spin system and to investigate the ergodicity status under coupling to the environment. Furthermore, we would like to investigate the same system with a larger number of sites to test the system size effect and to clarify the critical value of the parameter λ using finite-size scaling [25,26]. Previously, the 19-site triangular static Ising lattice was treated exactly using the the trace minimization algorithm [22]. The dynamics of entanglement in the 19-site XY system is currently under consideration, and by taking advantage of parallel computing, we can reach 34 spins by far.

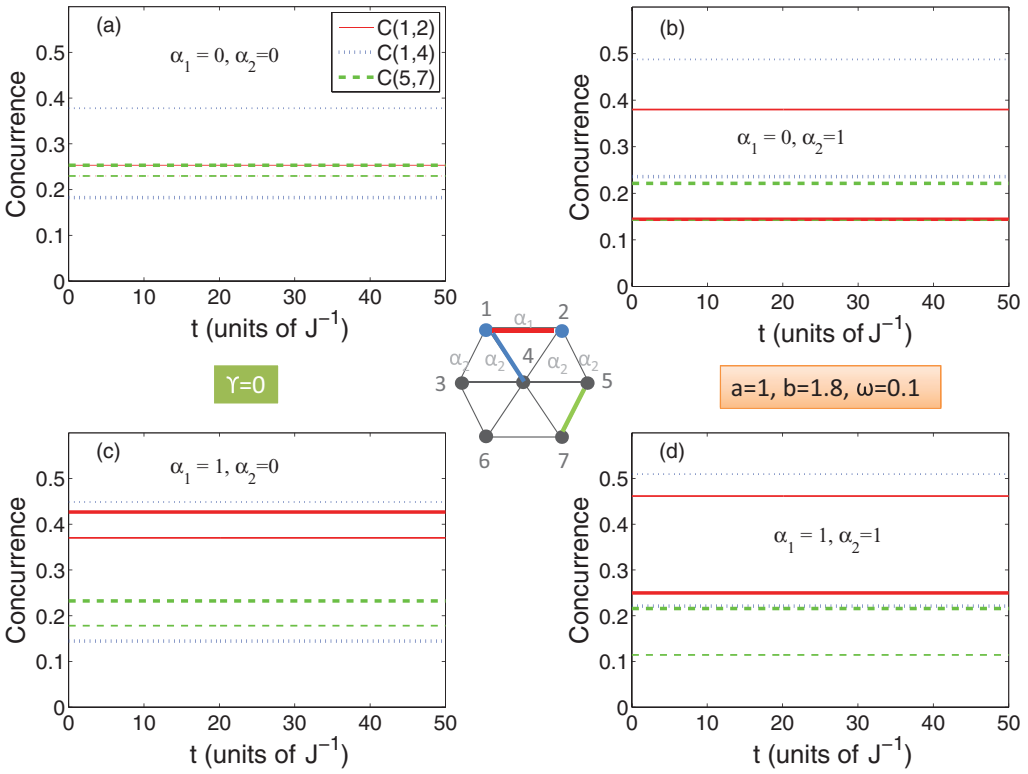

FIG. 25. (Color online) Dynamics of the concurrences $C(1,2), C(1,4), C(5,7)$ with double impurities at sites 1 and 2 for the two-dimensional isotropic XY lattice ($\gamma = 0$) in an exponential magnetic field where $a = 1$, $b = 1.8$, and $w = 0.1$. The straight (thicker) lines represent the equilibrium concurrences corresponding to constant magnetic field $h = 1.8$. The legend for all subfigures is as shown in (a).

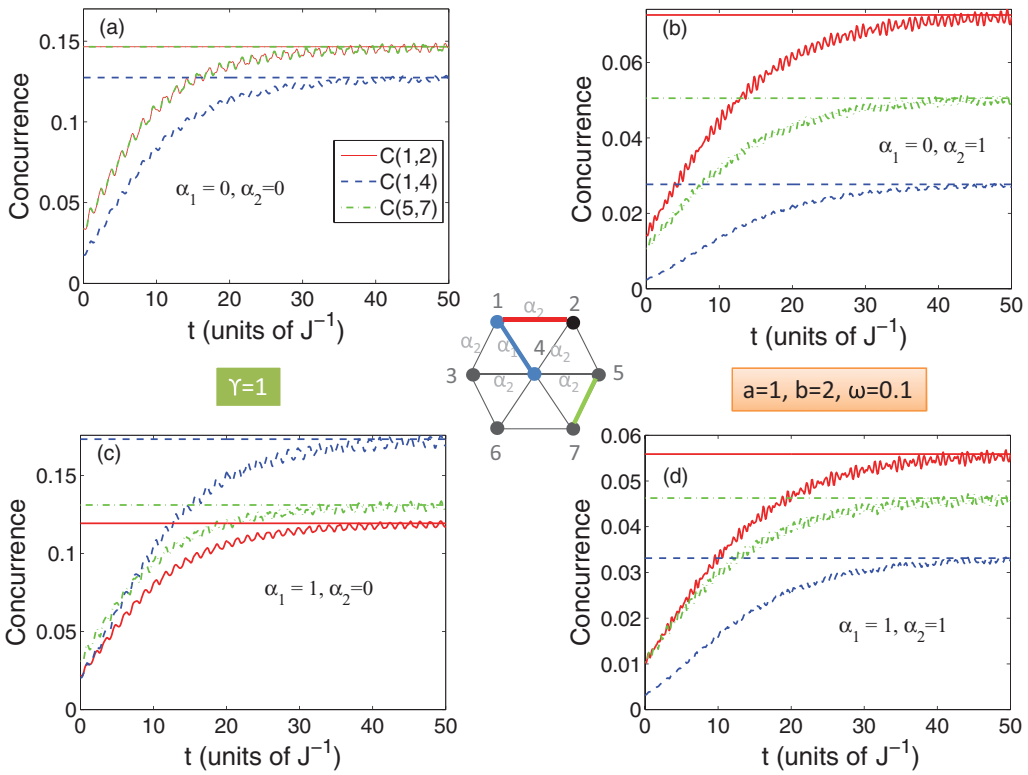

FIG. 26. (Color online) Dynamics of the concurrences $C(1,2), C(1,4), C(5,7)$ with double impurities at sites 1 and 4 for the two-dimensional Ising lattice ($\gamma = 1$) in an exponential magnetic field where $a = 1$, $b = 2$, and $w = 0.1$. The straight lines represent the equilibrium concurrences corresponding to constant magnetic field $h = 2$. The legend for all subfigures is as shown in (a).

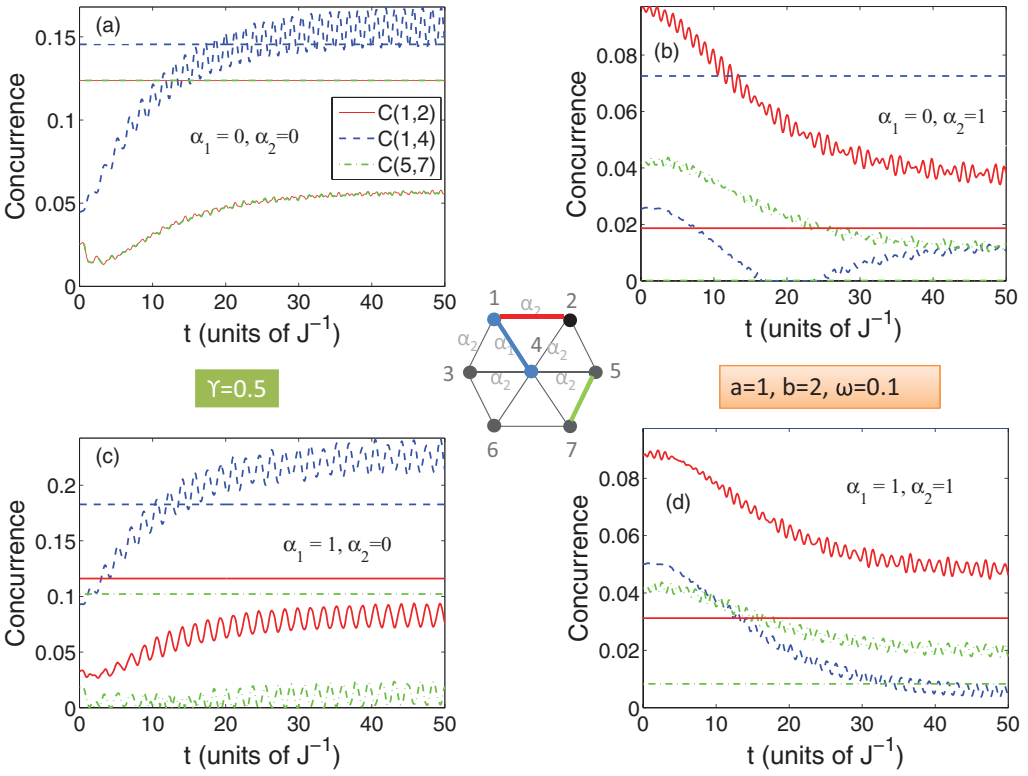

FIG. 27. (Color online) Dynamics of the concurrences $C(1,2), C(1,4), C(5,7)$ with double impurities at sites 1 and 4 for the two-dimensional partially anisotropic lattice ($\gamma = 0.5$) in an exponential magnetic field where $a = 1$, $b = 2$, and $w = 0.1$. The straight lines represent the equilibrium concurrences corresponding to constant magnetic field $h = 2$. The legend for all subfigures is as shown in (a).

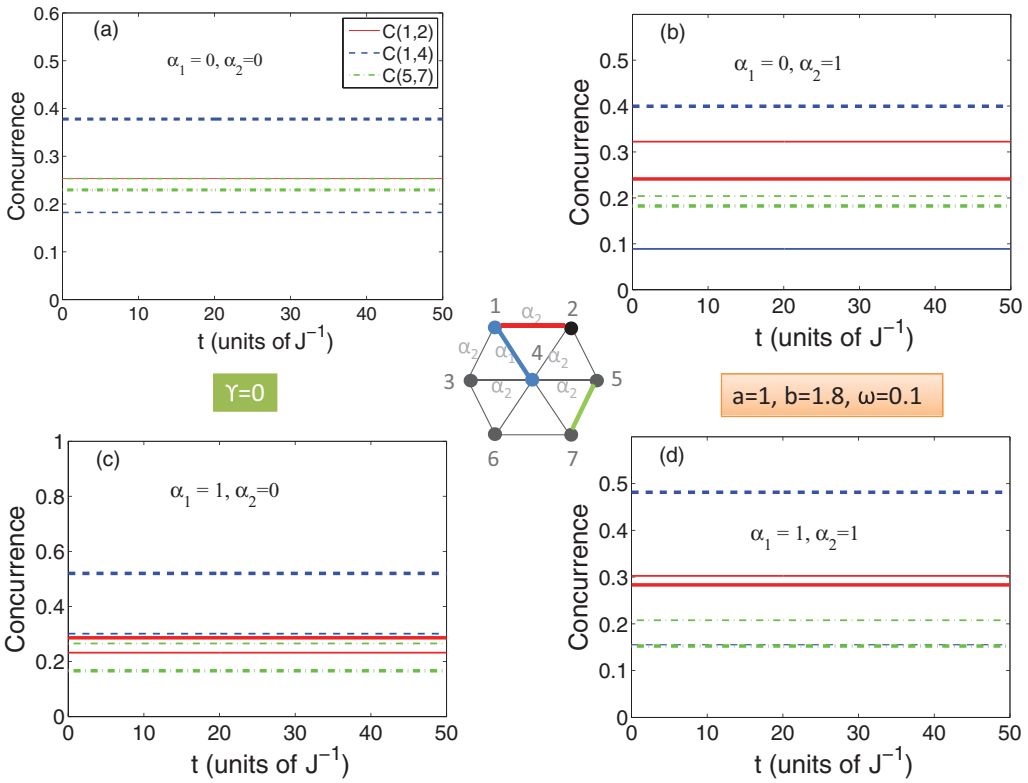

FIG. 28. (Color online) Dynamics of the concurrences $C(1,2), C(1,4), C(5,7)$ with double impurities at sites 1 and 4 for the two-dimensional isotropic XY lattice ($\gamma = 0$) in an exponential magnetic field where $a = 1$, $b = 1.8$, and $w = 0.1$. The straight (thicker) lines represent the equilibrium concurrences corresponding to constant magnetic field $h = 1.8$. The legend for all subfigures is as shown in (a).

ACKNOWLEDGMENTS

We are grateful to the Saudi NPST (Project No. 11-MAT1492-02) and the deanship of scientific research, King Saud University, for support. We are also grateful to the US Army Research Office for partial support of this work at Purdue University.

[1] A. Peres, *Quantum Theory: Concepts and Methods* (Kluwer, Dordrecht, 1993).
[2] M. Nielsen and I. Chuang, *Quantum Computation and Quantum Communication* (Cambridge University Press, Cambridge, UK, 2000).
[3] *The Physics of Quantum Information: Quantum Cryptography, Quantum Teleportation, Quantum Computing*, edited by D. Boumeester, A. Ekert, and A. Zeilinger (Springer, Berlin, 2000).
[4] S. L. Sondhi, S. M. Girvin, J. P. Carini, and D. Shahar, Rev. Mod. Phys. **69**, 315 (1997).
[5] T. J. Osborne and M. A. Nielsen, Phys. Rev. A **66**, 032110 (2002).
[6] Z. Huang, O. Osenda, and S. Kais, Phys. Lett. A **322**, 137 (2004).
[7] J. Zhang, F. M. Cucchietti, C. M. Chandrashekar, M. Laforest, C. A. Ryan, M. Ditty, A. Hubbard, J. K. Gamble, and R. Laflamme, Phys. Rev. A **79**, 012305 (2009).
[8] G. Sadiek, B. Alkurtass, and O. Aldossary, Phys. Rev. A **82**, 052337 (2010).
[9] B. Alkurtass, G. Sadiek, and S. Kais, Phys Rev. A **84**, 022314 (2011).
[10] J. A. Jones, Phys Rev. A **67**, 012317 (2003).
[11] H. K. Cummins, G. Llewellyn, and J. A. Jones, Phys Rev. A **67**, 042308 (2003).
[12] P. W. Shor, Phys. Rev. A **52**, R2493 (1995).
[13] D. Bacon, J. Kempe, D. A. Lidar, and K. B. Whaley, Phys. Rev. Lett. **85**, 1758 (2000).
[14] D. P. DiVincenzo, D. Bacon, J. Kempe, G. Burkard, and K. B. Whaley, Nature (London) **408**, 339 (2000).
[15] O. Osenda, Z. Huang, and S. Kais, Phys. Rev. A **67**, 062321 (2003).
[16] E. Barouch, Phys. Rev. A **2**, 1075 (1970).
[17] A. Sen(De), U. Sen, and M. Lewenstein, Phys Rev. A **70**, 060304 (2004).
[18] Z. Huang and S. Kais, Phys. Rev. A **73**, 022339 (2006).
[19] E. Lieb, T. Schultz, and D. Mattis, Ann. Phys. **16**, 407 (1961).
[20] S. Sachdev, *Quantum Phase Transitions* (Cambridge University Press, Cambridge, UK, 2001).
[21] Q. Xu, S. Kais, M. Naumov, and A. Sameh, Phys. Rev. A **81**, 022324 (2010).
[22] Q. Xu, G. Sadiek, and S. Kais, Phys. Rev. A **83**, 062312 (2011).
[23] A. Osterloh, L. Amico, G. Falci, and R. Fazio, Nature (London) **416**, 608 (2002).
[24] W. K. Wootters, Phys. Rev. Lett. **80**, 2245 (1998).
[25] S. Kais and P. Serra, *Advances in Chemical Physics* (Wiley, New York, 2003), Vol. 125, pp. 1–99.
[26] S. Kais, in *Reduced-Density-Matrix Mechanics—with Application to Many-Electron Atoms and Molecules*, Advances in Chemical Physics Vol. 134 (Wiley, New York, 2007), pp. 493–535.